An Efficient SSP-based Methodology for Assessing Climate Risks of a Large Credit Portfolio

Florian Bourgey, Emmanuel Gobet, Ying Jiao

An Efficient SSP-based Methodology for Assessing Climate Risks of a Large Credit Portfolio*

F. Bourgey† E. Gobet ‡ Y. Jiao §

July 31, 2024

Abstract

We examine climate-related exposure within a large credit portfolio, addressing transition and physical risks. We design a modeling methodology that begins with the Shared Socioeconomic Pathways (SSP) scenarios and ends with describing the losses of a portfolio of obligors. The SSP scenarios impact the physical risk of each obligor via a DICE-inspired damage function and their transition risk through production, requiring optimal adjustment. To achieve optimal production, the obligor optimizes various energy sources to align its greenhouse gas (GHG) emission trajectories with SSP objectives, while accounting for uncertainties in consumption trajectories. Ultimately, we obtain a Gaussian factor model whose dimension is of the order of the number of obligors. Two efficient dimension reduction methods (Polynomial Chaos Expansion and Principal Component Analysis) provide a fast and accurate method for analyzing credit portfolio losses.

Keywords: Climate Risks, Transitions Risks, Physical Risks, Credit Risk, Polynomial Chaos Expansion, Principal Component Analysis, Shared Socioeconomic Pathways, Optimal Production Profit.

MSC2020: 91G60, 91G40, 91B38, 86A08.

1 Introduction

Climate risk and financial impact. Facing the challenges of climate change, financial institutions are encouraged to shift their activities and investments toward a low-carbon economy. Under the Network for Greening the Financial System (NGFS), an increasing number of international banks have committed to the agreements made at the Conference of the Parties (COP 24) in Katowice in 2018, aiming to align their portfolios with the $\mathtt{CO_2}$ trajectories of the Paris Agreement. In other words, banks should incorporate the impact of climate change into the management of their asset portfolios. Notably, measuring and assessing the potential consequences of climate risks has become a key issue for financial institutions.

According to the Intergovernmental Panel on Climate Change (IPCC), $\mathtt{CO_2}$ and, more generally, greenhouse gas (GHG) emissions are among the main causes of global temperature increase. To achieve the idealized objective of limiting average warming to no higher than 1.5^oC, the IPCC summarizes [16] different potential macro-scenarios called Representative Concentration

*This research is supported by the *Chair Stress Test, RISK Management and Financial Steering* of the Foundation Ecole Polytechnique.

†Bloomberg, Quantitative Research, 731 Lexington Ave, New York, NY 10022, USA. Email: fbourgey@bloomberg.net

‡Centre de Mathématiques Appliquées (CMAP), CNRS, Ecole Polytechnique, Institut Polytechnique de Paris, France. Email: emmanuel.gobet@polytechnique.edu

§ISFA, Laboratoire SAF, Université Claude Bernard - Lyon 1, 69007 Lyon, France. Email: ying.jiao@univ-lyon1.fr

Pathways (RCP) to indicate possible GHG abatement scenarios. Based on more detailed socioeconomic criteria and factors, many other scenarios, known as Shared Socioeconomic Pathways (SSPs), have been proposed in the scientific literature, e.g., [29, 22]. These scenarios allow firms in different sectors and countries to anticipate and implement their mitigation strategy.

Climate risks in finance encompass two primary categories: physical and transition risks, as discussed in [9] and [2]. Physical risks entail immediate losses to companies due to shocks, especially as the severity and frequency of events like floods, heatwaves, and wildfires increase in extreme climate scenarios. Transition risks, on the other hand, result from firms shifting toward low-carbon production methods, profoundly influencing their future trajectory and impacting financial institutions and investors in the market. Modeling both risks remains a complex task with many uncertainties and limitations, but it is crucial for financial institutions granting loans to economic companies (obligors) to consider the transmission channels of climate-related risk drivers in the credit risk analysis of their portfolio.

Our study focuses on selected SSP scenarios, which describe future paths of GHG emissions across various sectors and temperature trajectories. We downscale these scenarios to individual obligors to model their adaptations (transition risks) and their impacts on physical risks. Subsequently, we aggregate this modeling at the level of the credit portfolio. The primary quantity of interest is the portfolio cumulative loss defined below in (1). The challenge we undertake is twofold: first, to design a robust and meaningful model; second, to efficiently and accurately solve and sample it, given the large number of obligors in the portfolio.

Literature on large portfolios and credit analysis. Financial institutions manage large portfolios consisting of n obligors, where n can be on the order of hundreds of thousands for major international banks. The cumulative loss is typically expressed as

$$\mathcal{L} = \sum_{i=1}^{n} \Lambda^i \times \mathbf{1}_{\{X^i \leq d^i\}} \tag{1}$$

where Λ^i (resp., d^i) represents the loss given default multiplied by the exposure at default (resp., the default barrier) of the ith obligor, X^i is the obligor's default-relevant variable, which also characterizes the dependence between obligors through correlated random factors. Modeling the marginal distributions of X^i and their dependence is crucial. In the current work, we explicitly model X^i and d^i in terms of the related SSP.

In the credit-risk literature neglecting climate risks, there exist two main approaches to describing the dependence of credit portfolios: the so-called bottom-up and top-down models. In the first approach, we start with the marginal distribution of each default time. Then, we specify the correlation structure, frequently utilizing copula models. For a comprehensive survey, refer to McNeil and Frey [23]. In the second approach, we focus directly on the cumulative loss process for credit portfolios to overcome the computational burden associated with portfolio size (see, e.g., [4]). In the first approach, when the size of a credit portfolio is very large, advanced numerical methods must be used as any naive Monte Carlo simulation becomes too time-consuming. Moreover, standard market models often impose a simplified dependence structure to facilitate computation. In factor models such as the Gaussian copula model, all obligors in the portfolio are correlated through one or several common macroeconomic or financial risk factors. Conditionally on these common factors, the default of the underlying companies is independent, as their heterogeneous factors are. A typical example is the one-factor Gaussian copula model of Li [21], where the loss is expressed as (1). In this model, $X^i = \rho^i Z + \sqrt{1-(\rho^i)^2}\varepsilon^i$ with Z and ε^i being independent standard normal random variables, and $\rho^i \in (-1, 1)$ being the correlation parameter. The default barrier d^i is deterministic.

We can also consider a multivariate default intensity model, generalizing the standard one-dimensional Cox model [18]. For a fixed horizon time $T > 0$, let $X^i = \int_0^T (\lambda_s + \lambda_s^i)\,\mathrm{d}s$ where λ and λ^i are non-negative processes representing the default intensity induced by common and

individual risk factors. The default barrier d^i is an independent exponential random variable. For other classical factor models in credit risk modeling and analysis, refer to [34] and [13].
In the credit-risk literature accounting for climate risks, the authors of [11] consider a multi-factor model called the Climate-Extended Risk Model (CERM) with several common risk factors, i.e., Z is a centered Gaussian random vector with a given correlation matrix. Our contribution is different as we consider a bottom-up modeling approach and additionally provide an efficient computational scheme to analyze the cumulative loss (1). To integrate the impact of climate risk into credit-sensitive firms and asset portfolios, [19] develops a structural model for defaultable bonds of companies exposed to transition risks. Unlike [19], which focuses on a single obligor, we model the credit risk of a large portfolio and also account for physical risks. Climate disaster-related events, such as Hurricane Harvey, have been incorporated using jump-diffusion processes to measure the impact of physical risks on the default probability of the housing sector, as demonstrated in [20]. In contrast to [20], our work focuses on a portfolio of obligors, accounting for dependence, and incorporates both physical and transition risks. Furthermore, adjustments to default probabilities and bond portfolio valuations are derived under various climate scenarios, based on the technological profiles of firms facing transition risks, as outlined in [3]. As a difference with [3], we focus on the credit risk of the portfolio rather than individual obligors. Additionally, our approach integrates both physical and transition risks into the modeling, and addresses related computational challenges.

Contributions of our paper. We propose a multi-default model that accounts for both transition and physical risks. Our contributions encompass three key aspects. Our comprehensive approach to modeling and computational methods is summarized in Figure 1.

Firstly, on the modeling front, starting from a target emission scenario such as one of the SSPs, we derive the obligor's transition efforts and strategies by considering a mix of different energy types, their emission factors, and associated costs; see Theorems 1, 2 and 3. These factors have a direct impact on the obligor's production methods and credit quality. The correlation structure among obligors is facilitated by introducing common systemic factors, akin to market factor models.

Secondly, in Section 3, we incorporate the projected costs associated with future physical risks that affect the obligor's overall value. This estimation draws on historical cost data and a modeling approach inspired by the Dynamic Integrated Model of Climate and Economy (DICE), reminiscent of Nordhaus' work [25, Eq. 5 p.10]. This approach acknowledges the inertia between GHG emissions and their subsequent effects on physical risks. Overall, our model offers a transparent mechanism for tracing how climate risks influence the creditworthiness of individual obligors. The marginal default probability for each obligor can be inferred using a bottom-up credit modeling approach.

Thirdly, we turn to computing credit risk metrics for large-scale portfolios using a top-down framework. Drawing inspiration from [6], we introduce an efficient numerical method based on Polynomial Chaos Expansions (PCE) for evaluating cumulative losses, see Section 5.3. However, our approach stands out by integrating dimension-reduction techniques specifically tailored to address climate risk.

As mentioned earlier, the correlation structure among obligors is established through a common systemic risk factor. We propose a method to reduce both the common and all idiosyncratic risk factors (amounting to $n+1$ factors) to just $2+\frac{1}{2}(M+1)(M+2)$ factors, where M is limited to a few units. This reduction is substantiated quantitatively through two main approaches: a) an analysis of eigenvalues via Principal Component Analysis (PCA), yielding two significant factors (see Section 5.2 and Proposition 5 for an L^1 error estimate), and b) a Polynomial Chaos Expansion applied to the limited systemic factors to perform a Gaussian approximation with $\frac{1}{2}(M+1)(M+2)$ terms. Additionally, we provide an error estimation for the truncated losses based on findings from [6, Theorems 2.6-7]. The improvement is significant especially for n large,

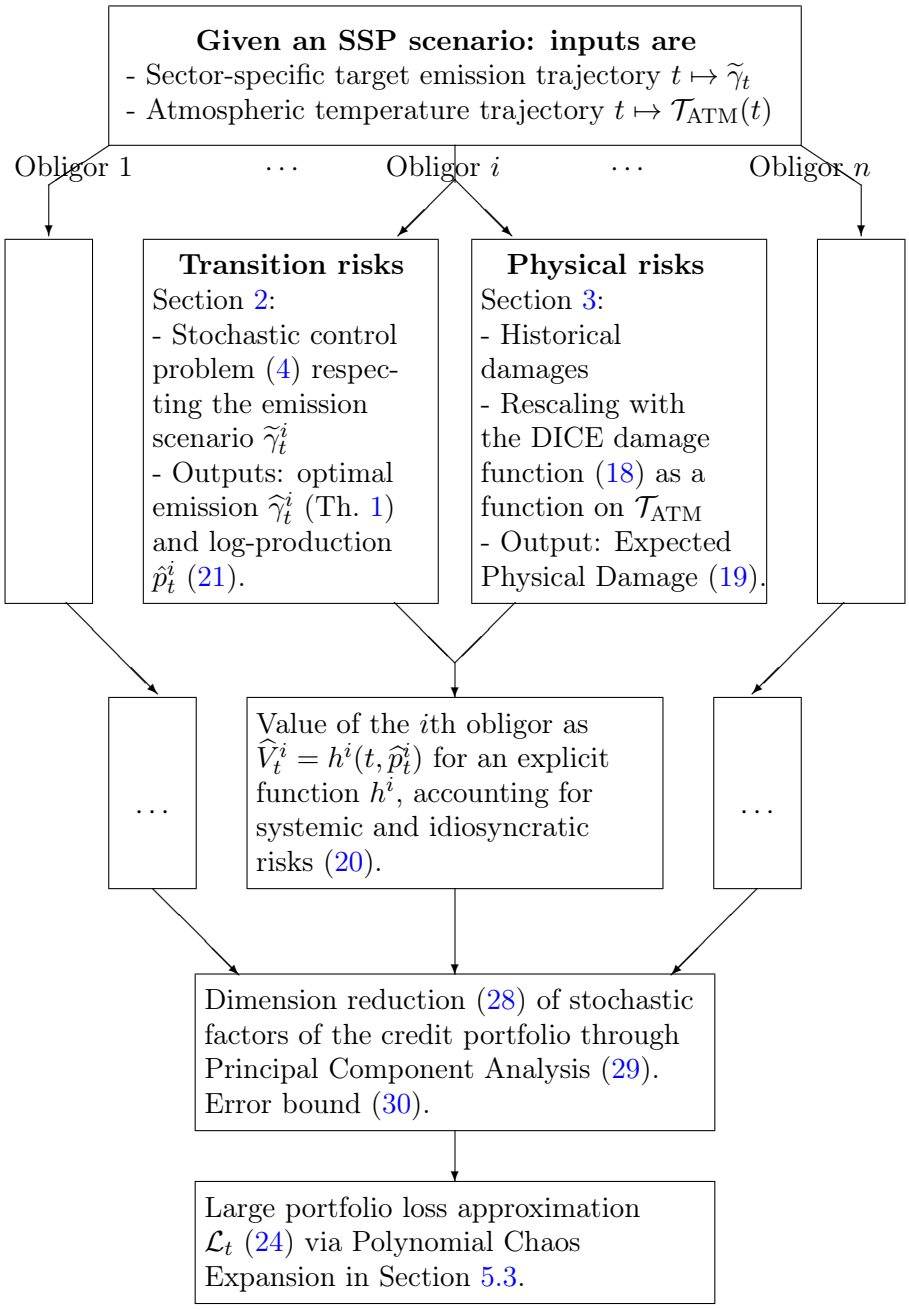

Figure 1: Diagram illustrating the analysis of the problem.

as discussed in Subsection 5.3. Our method has shown both accuracy and speed in practical applications, supported by numerical experiments.

The remainder of the paper is structured as follows. Section 2 addresses transition risk, deriving optimal emission strategies for an obligor navigating low-carbon mitigation transitions. Section 3 examines various potential physical risks and their impact on the obligor's value process. In Section 4, we quantify the combined impact of transition and physical risks on the obligor's credit quality, providing a semi-explicit formula for default probability in a special setting. Section 5 focuses on aggregating credit risks and calculating cumulative losses for large portfolios, introducing efficient numerical methods for computation. Technical details are deferred to the

Appendix.

2 Modeling the transition risk of each portfolio obligor

2.1 Overview of the approach

We consider a portfolio composed of $n \in \mathbb{N}^*$ companies whose production depends on their GHG emission levels measured in carbon dioxide equivalent $\mathtt{CO_2e}$ where $\mathtt{CO_2e}$ means that all GHG emissions have been converted into $\mathtt{CO_2}$ emissions. To allow comparison of the global warming of different gases, climate scientists use global warming potential (GWP) factors to convert one unit of a particular GHG to one unit of $\mathtt{CO_2}$. For example, methane $\mathtt{CH_4}$ has a GWP of about 27-30 over 100 years. Note that GHGs differ in their radiative efficiency (ability to absorb energy) and their lifetime (how long they stay in the atmosphere), see [28, Table 2.14] for a detailed table of these different GHG characteristics.

The companies aim to optimize their emission strategies following a low-carbon mitigation transition. Specifically, the ith obligor solves the infinite-horizon optimization problem

$$\mathcal{J}^i\left(\gamma^i_\bullet\right) = \mathbb{E}\left[\int_0^\infty e^{-rt}\left(\pi^i(P^i_t) - \mathcal{C}^i(\gamma^i_{\bullet,t}) - \ell^i_1(\gamma^i_{\bullet,t}) + \ell^i_2(\gamma^i_{\bullet,t})\right)\mathrm{d}t\right]$$

where

- P^i is the obligor's production assumed to depend on time and to be stochastic as it accounts for the demand uncertainty in goods. The production dynamics depends also on the energy power coming from different energy sources $\mathtt{e} \in \mathscr{E}^i$ where $\mathscr{E}^i$ is the set of all of the energy sources available to the ith obligor. The energy power is proportional to the vector of GHG emissions $\gamma^i_\bullet := (\gamma_\mathtt{e})_{\mathtt{e}\in\mathscr{E}^i}$, see Subsection 2.2 for details.
- π^i is a profit function and $r > 0$ is a discount factor.
- $\mathcal{C}^i(\gamma^i_\bullet)$ represents the cost of purchasing these different primary energies.
- National and international authorities penalize (resp., reward) companies emitting above (resp., below) an emission target, see below. This is encoded in the term $\ell^i_1(\gamma^i_\bullet)$ (resp., $\ell^i_2(\gamma^i_\bullet)$).

In our model, we do not consider any carbon compensation or offset, and we ignore carbon permits that could be traded in carbon markets. This extension is left to further research.

In the end, the optimal emission policy for the ith obligor is

$$\widehat{\gamma}^i_\bullet = \underset{\gamma^i_\bullet\in\mathcal{A}^i}{\arg\sup}\,\mathcal{J}^i\left(\gamma^i_\bullet\right),$$

where $\mathcal{A}^i$ is the set of admissible emission policies for the ith obligor. In this simplified model, we assume that companies are correlated through a common market factor but they do not interact with each other through the drift coefficient.

Below, we describe each step and establish that, under suitable model hypotheses, there exists a unique emission policy for each obligor.

2.2 Modeling the link between GHG emissions and production

Energy sources: GHG emissions, emission factors, and cost. According to the U.S. Energy Information Administration (EIA)[1], the different energy sources used by the U.S. industrial sector are: natural gas, petroleum, electricity, renewable sources (mainly biomass), and

[1] https://www.eia.gov/energyexplained/use-of-energy/industry.php

coal. Depending on how and where these energy sources are produced, their climate impact and price are different. For example, most companies purchase electricity from electric utilities, independent power producers, or possibly produce electricity for their own use with solar panels. Electricity can be produced from nuclear energy (nuclear power plant), renewable energy (wind, hydroelectric power plant, photovoltaic), fossil energy (oil, coal-fired power plant) or a combination of nuclear/renewable/fossil energies. Depending on where the obligor operates and its choice of suppliers, the electricity might be produced from a different electric mix. To illustrate this, in Table 1, we show an example of three different UK Electricity Suppliers as of 2022. Observe for example that electricity produced from nuclear energy (resp., gas) is 63.1% (resp., 15.1%) for EDF Energy and 7.0% (resp., 74.0%) for Utilita.

Supplier	Coal	Gas	Nuclear	Renewable	Other	Emission factor ($\mathtt{kgCO_2e}$ per $\mathtt{kWh}$)
Utilita	9.0	74.0	7.0	3.0	8.0	0.429
e.on	2.0	16.1	1.5	78.8	1.6	0.093
EDF Energy	1.6	15.1	63.1	19.0	1.2	0.082
Bulb	0	0	0	100.0	0	≈ 0

Table 1: Fuel Mix (in %) of some of the UK Domestic Electricity Suppliers as of 2022. Those values are taken from https://electricityinfo.org/fuel-mix-of-uk-domestic-electricity-suppliers/. We assume here that $1\mathtt{kgCO_2e} \approx 1\mathtt{kgCO_2}$ for electricity production. Note that because of The Electricity (Fuel Mix Disclosure) Regulations Act of 2005, electric suppliers are obligated to provide details of the mix of fuels used to produce electricity https://www.legislation.gov.uk/uksi/2005/391/contents/made.

The last column of Table 1 is the so-called emission factor (sometimes called emission intensity or carbon output rate) [2]. It quantifies how much GHG emissions (measured in $\mathtt{CO_2e}$) are released when consuming 1 $\mathtt{kWh}$ of a particular energy source $\mathtt{e}$. In Table 2, we report some of these values. Observe that the emission factor for electricity produced from coal is about $\frac{0.820}{0.012} \approx 68$ times higher than electricity produced from nuclear energy. Emission factors for world countries as of 2022 are reported in [15].

Source of Energy	Emission factors ($\mathtt{kgCO_2e}$ per $\mathtt{kWh}$)
Electricity (Coal)	0.820
Electricity (Gas)	0.490
Electricity (Wind)	0.011
Electricity (Nuclear)	0.012
Electricity (Hydro)	0.024
Charcoal	0.403
Crude Oil	0.264
Natural Gas	0.202

Table 2: A few examples of emission factors. For the emission factors from electricity generation, we report the median values of the lifecycle emissions from [32, Table A.III.2]. For the others, we report the default emission factors of [12, Table 2.2]. We have used the conversion $1\mathtt{kg/TJ} = \frac{18}{5} \times 10^{-6} \times 1\mathtt{kg/kWh}$ where $1\mathtt{TJ}$ is one tera joule. Those values are also reported at https://ourworldindata.org/grapher/carbon-dioxide-emissions-factor

We also stress that countries have different energy mix profiles. For example, in Figure 2, we plot the energy mix for China, the USA, and France in 2022. The share of electricity produced from nuclear energy is 63% for France, 5% for China, 18% for the USA, while when produced

[2] terminology from https://ember-climate.org/insights/research/european-electricity-review-2022/ and https://www.eia.gov/tools/glossary/index.php?id=c

from coal it is 1% for France, 61% for China, and 19% for the USA.

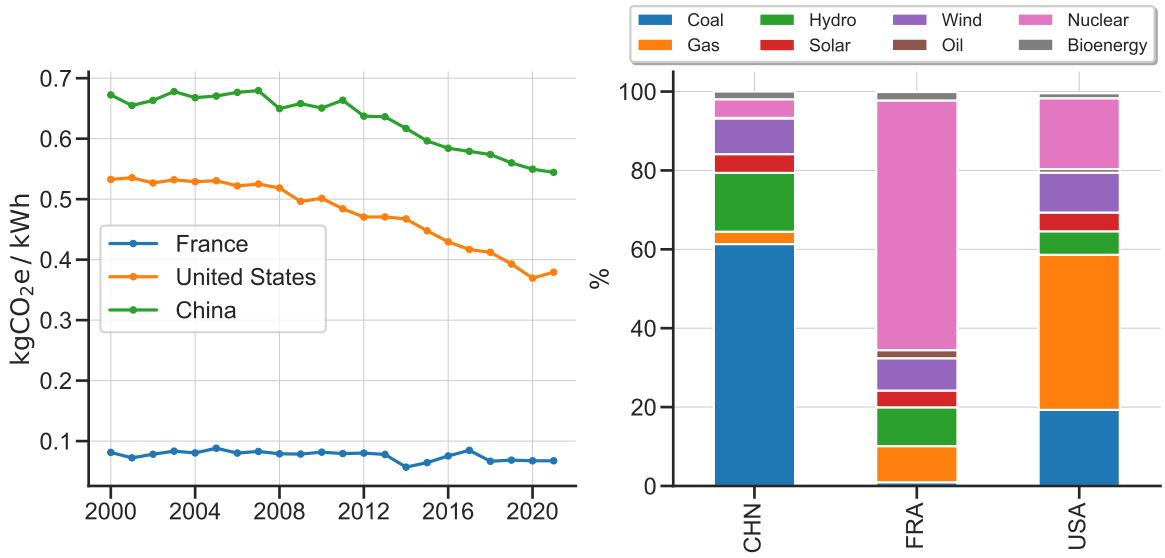

Figure 2: Left: emission factors of electricity in $\texttt{kgCO}_2\texttt{e/kWh}$ as a function of time for France, the USA, and China. Right: Bar plots of the electricity mix as of 2022 for the same countries. Data taken from [30].

Notation. In our model, we denote by $\mathscr{E}^{\text{all}}$ the set of all possible energy sources[3] an obligor can use for its production:

$$\begin{aligned}\mathscr{E}^{\text{all}} := \{&\text{Coal consumption, Coal coke net imports, Petroleum consumption,}\\ &\text{Dry natural gas consumption, Nuclear electricity net generation,}\\ &\text{Hydroelectricity net generation, Geothermal electricity net generation,}\\ &\text{Solar thermal and photovoltaic electricity net generation,}\\ &\text{Wind electricity net generation, Electricity net imports, ...}\}.\end{aligned}$$

We let $\mathscr{E}^i \subseteq \mathscr{E}^{\text{all}}$ be the energy sources available to the ith obligor. Notice the dependence of i for $\mathscr{E}^i$ as the set of all available energy sources might differ from one obligor to the other (different locations, different suppliers, etc). An obligor is unlikely to have access to all possible energy sources $\mathscr{E}^{\text{all}}$ and to use all available energy sources $\mathscr{E}^i$. This fact will be materialized in the constraint set $\mathcal{G}^i$, see (6) in Subsection 2.3. We stress that we are not attempting to optimize the selection of energy sources $(\mathtt{e})_{\mathtt{e}\in\mathscr{E}^i}$, but rather to optimize the obligor's emissions $(\gamma_{\mathtt{e}})_{\mathtt{e}\in\mathscr{E}^i}$.

Two features characterize an energy source $\mathtt{e} \in \mathscr{E}^i$:

- the price $\alpha^i_{\mathtt{e},t} > 0$ per unit of $\mathtt{e}$-energy consumed by the ith obligor at time t. The price may differ from one obligor to the other as it depends on the location of the obligor's offices, factories, and its access to related energy supply companies and their rates. We assume that the price is a deterministic function of time [4]. Its unit is $\texttt{USD/kWh}$. In Figure 3, we plot the yearly U.S. average prices of gasoline, gas, and electricity from 1978-79 to 2023.

- the power/$\texttt{CO}_2\texttt{e}$ ratio $\theta^i_{\mathtt{e},t} > 0$. It corresponds to the average production rate for each energy $\mathtt{e}$, i.e., the quotient of the total equivalent power production with respect to the

[3] It corresponds to the list of energy sources for "Primary Energy Consumption" in the EIA's glossary https://www.eia.gov/tools/glossary.

[4] Ideally, the price $\alpha_{\mathtt{e},t}$ should depend on the future scenario pathway considered. Electric price scenarios for some sectors are available in the AR6 database https://data.ene.iiasa.ac.at/ar6

equivalent $\mathtt{CO_2}$ emission from using $\mathtt{e}$. Its unit is $\mathtt{kW/kgCO_2e}$. It equals the inverse of the emission factor (previously described), divided by one hour. These power/$\mathtt{CO_2e}$ ratios may depend on i because companies may differ in their geographic zones and countries with different electricity mixes, as illustrated in Figure 2. We assume that each $t \mapsto \theta^i_{\mathtt{e},t}$ is a deterministic function of time.

For every obligor, there exists a trade-off between price and emission factor depending on how "green" the obligor is. An obligor might want to pay more for using "cleaner" energy sources.

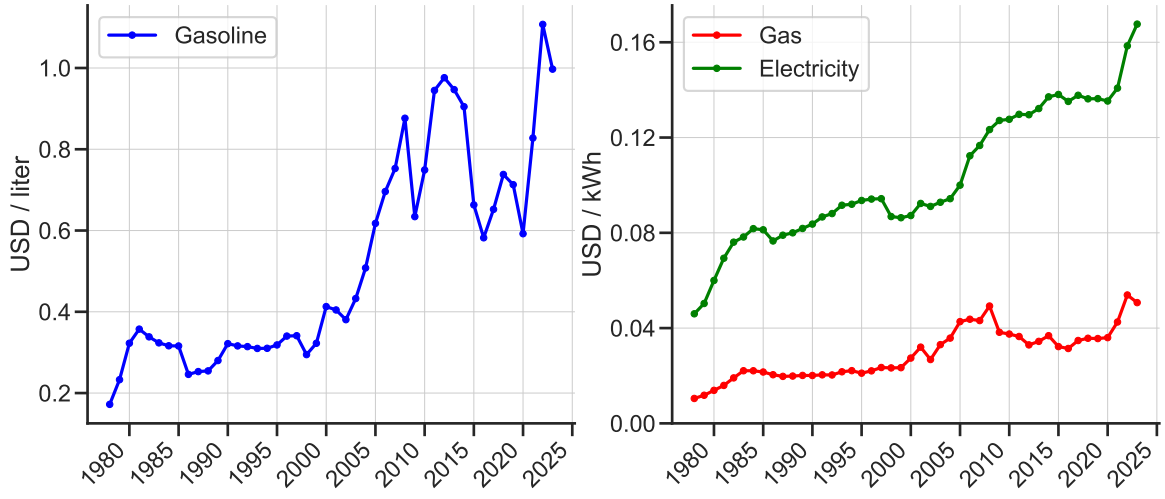

Figure 3: Left: Yearly US average price of Gasoline in $\mathtt{USD}$/liter. Right: Yearly US average prices of household gas and electricity in $\mathtt{USD/kWh}$. Source: U.S. Bureau of Labor Statistics.

We denote by $\gamma^i_{\bullet,t} := (\gamma^i_{\mathtt{e},t})_{\mathtt{e}\in\mathscr{E}^i}$ the vector of instantaneous GHG emissions for the ith obligor coming from each of the primary energy sources $\mathtt{e} \in \mathscr{E}^i$. Its unit is $\mathtt{kgCO_2e}$. With our notations, the instantaneous energy (in $\mathtt{kWh}$) coming from $\mathtt{e}$ consumed during a small interval $[t, t + \mathrm{d}t]$ (in hours $\mathtt{h}$) is then

$$\theta^i_{\mathtt{e},t} \times \gamma^i_{\mathtt{e},t}\, \mathrm{d}t.$$

The cost (in $\mathtt{USD}$) of consuming such energy is

$$\alpha^i_{\mathtt{e},t} \times \theta^i_{\mathtt{e},t} \times \gamma^i_{\mathtt{e},t}\, \mathrm{d}t,$$

while the cost (in $\mathtt{USD}$) of consuming energy coming from all sources $\mathtt{e} \in \mathscr{E}^i$ is

$$\sum_{\mathtt{e}\in\mathscr{E}^i} \alpha^i_{\mathtt{e},t} \times \theta^i_{\mathtt{e},t} \times \gamma^i_{\mathtt{e},t}\, \mathrm{d}t =: \alpha^{i,\theta}_{\bullet,t} \cdot \gamma^i_{\bullet,t}\, \mathrm{d}t$$

where we have introduced the short-hand notation

$$\alpha^{i,\theta}_{\bullet,t} := (\alpha^i_{\mathtt{e},t} \times \theta^i_{\mathtt{e},t})_{\mathtt{e}\in\mathscr{E}^i},$$

and $\cdot$ denotes the scalar product. In addition, to account for the limited amount of energy available at a given date, we add a quadratic term that captures the fact that marginal energy cost is increasing with the demand. Introducing the notations,

$$\beta^{i,\theta}_{\bullet,t} := \left(\beta^i_{\mathtt{e},t} \times (\theta^i_{\mathtt{e},t})^2\right)_{\mathtt{e}\in\mathscr{E}^i}, \qquad (\gamma^2)^i_{\bullet,t} := ((\gamma^i_{\mathtt{e},t})^2)_{\mathtt{e}\in\mathscr{E}^i},$$

the total energy cost over the interval $[t, t + \mathrm{d}t]$ writes as

$$\begin{aligned}\mathcal{C}^i(\gamma^i_{\bullet,t})\, \mathrm{d}t &= \sum_{\mathtt{e}\in\mathscr{E}^i} \left(\alpha^i_{\mathtt{e},t} \times \left(\theta^i_{\mathtt{e},t} \times \gamma^i_{\mathtt{e},t}\right) + \beta^i_{\mathtt{e},t} \times \left(\theta^i_{\mathtt{e},t} \times \gamma^i_{\mathtt{e},t}\right)^2\right)\, \mathrm{d}t \\ &= \left(\alpha^{i,\theta}_{\bullet,t} \cdot \gamma^i_{\bullet,t} + \beta^{i,\theta}_{\bullet,t} \cdot (\gamma^2)^i_{\bullet,t}\right)\, \mathrm{d}t\end{aligned}$$

where $t \mapsto \alpha^i_{\mathsf{e},t}$ and $t \mapsto \beta^i_{\mathsf{e},t}$ (and thus $t \mapsto \alpha^{i,\theta}_{\mathsf{e},t}$ and $t \mapsto \beta^{i,\theta}_{\mathsf{e},t}$) are strictly positive and deterministic measurable functions of time for any $\mathsf{e} \in \mathscr{E}^i$.

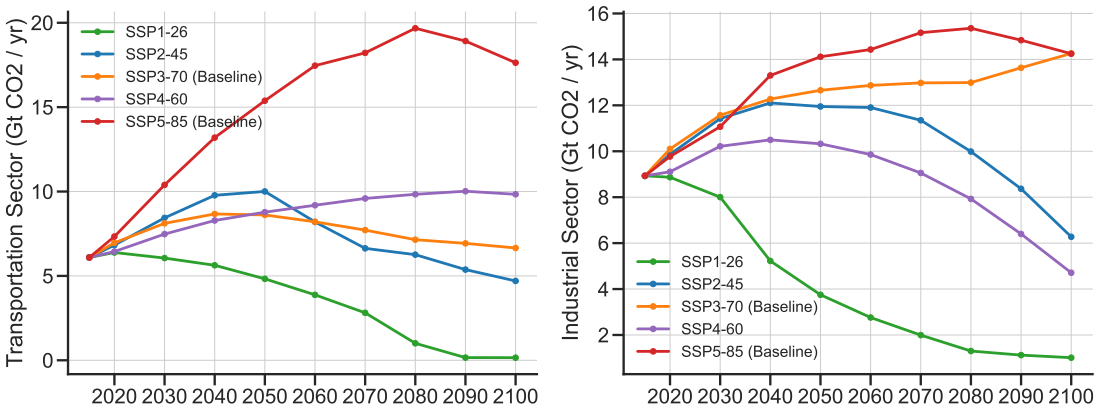

Figure 4: $\mathtt{CO_2}$ emissions in some of the CIMP6 Scenarios for the transportation (left figure) and industrial (right figure) sectors. See the AR6 Scenario Explorer and Databased at https://data.ene.iiasa.ac.at/ar6/.

Global GHG emissions. Using the previous notations, the total GHG emissions is

$$\sum_{\mathsf{e}\in\mathscr{E}^i} \gamma^i_{\mathsf{e},t} = \mathbf{1}\cdot\gamma^i_{\bullet,t}$$

where $\mathbf{1}$ is a vector with unit components in the appropriate dimension equal to $|\mathscr{E}^i|$.

Let $\widetilde{\gamma}^i = (\widetilde{\gamma}^i_t,\, t \geq 0)$ be a carbon emission benchmark (e.g., an SSP of a certain sector to which the i^{th} obligor belongs to), which is supposed to be a deterministic and measurable function with respect to time. See Figure 4 for such emission benchmarks. At time t, the obligor is:

- penalized if its global emission is above $\widetilde{\gamma}^i_t$ through $\ell^i_1\left(\mathbf{1}\cdot\gamma^i_{\bullet,t} - \widetilde{\gamma}^i_t\right)$ where ℓ^i_1 is a non-decreasing continuous function,
- rewarded if its global emission is below $\widetilde{\gamma}^i_t$ through $\ell^i_2\left(\widetilde{\gamma}^i_t - \mathbf{1}\cdot\gamma^i_{\bullet,t}\right)$ where ℓ^i_2 is another non-decreasing continuous function.

We further assume that ℓ^i_1, ℓ^i_2 have at most a quadratic growth at infinity. They correspond to national or international policies aimed at incentivizing the reduction of GHG emissions through the establishment of specific quantitative targets.

Example 1. The functions ℓ^i can be taken as

$$\ell^i_1(x) = \omega^i_1\, x^2_+, \qquad\qquad \ell^i_2(x) = \omega^i_2\, x^2_+,$$

where $x_+ = \max(x, 0)$, and $\omega^i_1, \omega^i_2 \geq 0$ are constant parameters representing respectively the penalty and reward forces. We choose a quadratic penalty (resp., reward) function to accentuate large values of over-emission (resp., under-emission) compared to the benchmark emission scenario. This example is further investigated in Theorems 3 and 4. This results in a convex problem that allows for an explicit solution for each obligor and can be solved numerically with fast algorithms for all obligors in the portfolio.

Example 2. The functions ℓ^i can be taken as

$$\ell^i_1(x) = \omega^i_1\, x^2_+, \qquad\qquad \ell^i_2(x) = \omega^i_2\, x_+.$$

Here, the reward function has a linear growth rate. Compared to the previous example, there is less incentive to pollute less though the cost of polluting remains the same.

Production dynamics and profit function. We consider the special model where the profit function is given by

$$\pi^i(x) = \mathrm{AP}^i \times \log(x),$$

where AP^i is a given average price.

To define the stochastic model for the production, consider a filtered probability space $(\Omega, \mathcal{F}, \mathbb{F} = (\mathcal{F}_t)_{t\geq 0}, \mathbb{P})$ on which is defined $n+1$ independent standard Brownian motions $B, B^1, \ldots, B^n$. Given the logarithmic nature of the profit function, we directly model the log-production $p_t^i = \log(P_t^i)$ as a linear stochastic differential equation

$$\begin{aligned} \mathrm{d}p_t^i &= \mu^i(t, p_t^i, \gamma_{\bullet,t}^i)\,\mathrm{d}t + \sigma^i\,\mathrm{d}W_t^i, \\ \mu^i(t, p, \gamma_{\bullet,t}^i) &= a^i - b^i p + \sum_{\mathsf{e}\in\mathscr{E}^i} c_{\mathsf{e}}^i \times \gamma_{\mathsf{e},t}^i \times \theta_{\mathsf{e},t}^i \\ &= a^i - b^i p + c_\bullet^{i,\theta} \cdot \gamma_{\bullet,t}^i, \end{aligned} \tag{2}$$

where we have introduced

$$c_\bullet^{i,\theta} := (c_{\mathsf{e}}^i \times \theta_{\mathsf{e},t}^i)_{\mathsf{e}\in\mathscr{E}^i}$$

and

$$\mathrm{d}W_t^i = \rho^i\,\mathrm{d}B_t + \sqrt{1-(\rho^i)^2}\,\mathrm{d}B_t^i \tag{3}$$

with correlations $\rho^i \in (-1, 1)$. B reads as a systemic risk factor and the $(B^i)_{1\leq i\leq n}$ as independent idiosyncratic risk factors. We further assume that $\sigma^i > 0$.

In (2), the coefficient $a^i \geq 0$ represents an average production level, $b^i \geq 0$ is a mean-reverting parameter and c_{e}^i measures the obligor's energy consumption dependence on e. Making c_{e}^i depend on e serves as a means to convey that, from the perspective of the ith obligor, it is possible to interchange energy sources, even though the power consumption $\gamma_{\mathsf{e}}^i \times \theta_{\mathsf{e}}^i$ remains the same. To illustrate this concept, consider the straightforward example of hydroelectric power generation and fuel usage for vehicle transportation.

2.3 The obligor's optimization plan

Each obligor aims to optimize its emission level under the double objectives of maximizing its production profit and respecting the emission mitigation scenario. Mathematically, it corresponds to

$$\widehat{\gamma}_\bullet^i := \operatorname*{arg\,sup}_{\gamma_\bullet^i\in\mathcal{A}^i} \mathcal{J}^i\left(\gamma_\bullet^i\right), \tag{4}$$

$$\begin{aligned} \mathcal{J}^i\left(\gamma_\bullet^i\right) := \mathbb{E}\Bigg[\int_0^\infty e^{-rt}\Big(&\mathrm{AP}^i\, p_t^i - \alpha_{\bullet,t}^{i,\theta}\cdot\gamma_{\bullet,t}^i - \beta_{\bullet,t}^{i,\theta}\cdot(\gamma^2)_{\bullet,t}^i \\ &- \ell_1^i\left(\mathbf{1}\cdot\gamma_{\bullet,t}^i - \widetilde{\gamma}_t^i\right) + \ell_2^i\left(\widetilde{\gamma}_t^i - \mathbf{1}\cdot\gamma_{\bullet,t}^i\right)\Big)\mathrm{d}t\Bigg], \end{aligned} \tag{5}$$

where $r > 0$ is a constant positive discount rate. The admissible stochastic control set $\mathcal{A}^i$ contains all progressively measurable processes $\gamma_\bullet^i$ valued in

$$\prod_{t\geq 0} \mathcal{G}_{\bullet,t}^i \quad \text{with} \quad \mathcal{G}_{\bullet,t}^i = \prod_{\mathsf{e}\in\mathscr{E}^i} [0, \lambda_{\mathsf{e},t}^{\max}] \tag{6}$$

where the function $t \mapsto \lambda_{\mathsf{e},t}^{\max}$ is measurable.

Mathematically, what is important is that the set $\mathcal{G}_{\bullet,t}^i$ is a closed, bounded, and non-empty subset [5] of $[0, +\infty)^{|\mathscr{E}^i|}$.

[5] Allowing for unbounded $\mathcal{G}_t^i$ is presumably possible but would lead to extra technicalities that are not central to our work. Furthermore, on the application side, restricting to bounded emissions is natural.

We assume that the following integrability condition holds: there exists $\eta \in (0, r)$ such that

$$\int_0^\infty e^{-\eta t} \sup_{\gamma^i_{\bullet,t} \in \mathcal{G}^i_{\bullet,t}} |\gamma^i_{\bullet,t}|^2 \mathrm{d}t < +\infty. \tag{7}$$

In view of (6), the condition writes $\int_0^\infty e^{-\eta t} \sup_{\mathsf{e} \in \mathscr{E}^i} (\lambda^{\max}_{\mathsf{e},t})^2 \mathrm{d}t < +\infty$.

2.4 Existence and uniqueness of an optimal emission

We now characterize the solution $\widehat{\gamma}^i_\bullet$ to the optimization problem (4).

Theorem 1. *Let $i \in \{1, \cdots, n\}$ and for any $\gamma_{\bullet,t}$, define*

$$f^i_t(\gamma^i_{\bullet,t}) := \frac{\mathrm{AP}^i}{r + b^i} c^{i,\theta}_\bullet \cdot \gamma^i_{\bullet,t} - \alpha^{i,\theta}_{\bullet,t} \cdot \gamma^i_{\bullet,t} - \beta^{i,\theta}_{\bullet,t} \cdot (\gamma^2)^i_{\bullet,t} - \ell^i_1\big(\mathbf{1} \cdot \gamma^i_{\bullet,t} - \widetilde{\gamma}^i_t\big) + \ell^i_2\big(\widetilde{\gamma}^i_t - \mathbf{1} \cdot \gamma^i_{\bullet,t}\big). \tag{8}$$

Assume that

- *the benchmark global emission $t \mapsto \widetilde{\gamma}^i_t$ is such that*

$$\int_0^\infty e^{-\eta t} |\widetilde{\gamma}^i_t|^2 \mathrm{d}t < +\infty, \tag{9}$$

- *there exists a $\widehat{\gamma}^i_{\bullet,t} \in \mathcal{G}^i_{\bullet,t}$ maximizing $f^i_t(\cdot)$.*

Then, this maximizer solves the optimal stochastic control problem (4).

Theorem 2. *Assume that (9) holds, that $\gamma^i_{\bullet,t} \mapsto f^i_t(\gamma^i_{\bullet,t})$ is continuous and strictly concave. Then, there exists a unique $\widehat{\gamma}^i_{\bullet,t} \in \mathcal{G}^i_{\bullet,t}$ maximizing $f^i_t(\cdot)$ and thus solving the optimization problem (4).*

The main advantage of the setting of Theorem 2 compared to that of Theorem 1 is algorithmic, because, in the above *concave case*, we can make use of fast algorithms to compute the maximizer of $f^i_t(\cdot)$, (see, e.g., the projected gradient descent algorithm exposed in Remark 7).

Theorem 3. *Consider the loss functions of Example 1, i.e., $\ell^i_1(x) = \omega^i_1 (x_+)^2$ and $\ell^i_2(x) = \omega^i_2 (x_+)^2$. Then, when $\omega^i_2 \big(\mathbf{1} \cdot \frac{1}{\beta^{i,\theta}_{\bullet,t}}\big) < 1$ for any $t \geq 0$, the assumptions of Theorem 2 are satisfied.*

Note that the loss functions of Example 2 do not allow to retrieve a concave problem: as the reader can easily check, this is mainly due to the fact that $g(z) : z \mapsto z^2 - c z_+$ (with $c > 0$) is not a convex function (indeed, $g(\epsilon) + g(-\epsilon) < 2g(0)$ for a small enough $\epsilon > 0$). Despite this lack of convexity, the conditions of Theorem 1 apply: indeed, the function $\gamma^i_{\bullet,t} \mapsto f^i_t(\gamma^i_{\bullet,t})$ is continuous on a compact set $\mathcal{G}^i_t$ and, thus, admits a maximizer. However, the uniqueness is not guaranteed.

Proof of Theorem 1. To alleviate notation, we omit the index i. Let $\gamma_\bullet = (\gamma_\mathsf{e})_{\mathsf{e} \in \mathscr{E}} \in \mathcal{A}$ be an admissible strategy to the problem (5). Then, the difference $J(\widehat{\gamma}_\bullet) - J(\gamma_\bullet)$ equals

$$\mathbb{E}\bigg[\int_0^\infty e^{-rt} \Big(\mathrm{AP}\big(\widehat{p}_t - p_t\big) - \alpha^\theta_{\bullet,t} \cdot \big(\widehat{\gamma}_{\bullet,t} - \gamma_{\bullet,t}\big) - \beta^\theta_{\bullet,t} \cdot \big((\widehat{\gamma}^2)_{\bullet,t} - (\gamma^2)_{\bullet,t}\big) \\ - \ell_1(\mathbf{1} \cdot \widehat{\gamma}_{\bullet,t} - \widetilde{\gamma}_t) + \ell_1(\mathbf{1} \cdot \gamma_{\bullet,t} - \widetilde{\gamma}_t) + \ell_2(\widetilde{\gamma}_t - \mathbf{1} \cdot \widehat{\gamma}_{\bullet,t}) - \ell_2(\widetilde{\gamma}_t - \mathbf{1} \cdot \gamma_{\bullet,t}) \Big) \mathrm{d}t \bigg] \tag{10}$$

where $\widehat{p}_t$ is given by

$$\mathrm{d}\widehat{p}_t = (a - b\widehat{p}_t + c^\theta_\bullet \cdot \widehat{\gamma}_{\bullet,t})\mathrm{d}t + \sigma \mathrm{d}W_t, \qquad \widehat{p}_0 = p_0. \tag{11}$$

By Ito's formula, we have

$$\mathrm{d}\big(e^{-rt}(\widehat{p}_t - p_t)\big) = e^{-rt}\Big(- (b + r)(\widehat{p}_t - p_t) + c^\theta_\bullet \cdot (\widehat{\gamma}_{\bullet,t} - \gamma_{\bullet,t})\Big)\mathrm{d}t. \tag{12}$$

Since $\gamma_\bullet \in \mathcal{A}$, we have

$$\mathbb{E}\left[\Big(\int_0^\infty e^{-\eta t}|c_\bullet^\theta \cdot \gamma_{\bullet,t}|\mathrm{d}t\Big)^2\right] \le \Big(\int_0^\infty (e^{-\eta t/2})^2 \mathrm{d}t\Big)\ \mathbb{E}\left[\int_0^\infty (e^{-\eta t/2}|c_\bullet^\theta \cdot \gamma_{\bullet,t}|)^2 \mathrm{d}t\right]$$
$$\le \frac{|c_\bullet^\theta|^2}{\eta}\mathbb{E}\left[\int_0^\infty e^{-\eta t}|\gamma_{\bullet,t}|^2 \mathrm{d}t\right] < +\infty$$

using the integrability condition (7). Therefore, the integral $\int_0^\infty e^{-\eta t}|c_\bullet^\theta \cdot \gamma_{\bullet,t}|\mathrm{d}t$ is finite almost surely; the same holds obviously for $\widehat{\gamma}_\bullet$. By solving the equation (11), we get

$$\widehat{p}_t - p_t = \int_0^t e^{-b(t-s)} c_\bullet^\theta \cdot (\widehat{\gamma}_{\bullet,s} - \gamma_{\bullet,s})\mathrm{d}s,$$
$$|e^{-rt}(\widehat{p}_t - p_t)| \le e^{(\eta - r)t}\int_0^t e^{-\eta s}|c_\bullet^\theta \cdot (\widehat{\gamma}_{\bullet,s} - \gamma_{\bullet,s})|\mathrm{d}s$$

using $b \ge 0$. Hence, since $r > \eta$,

$$\lim_{t\to+\infty} e^{-rt}(\widehat{p}_t - p_t) = 0, \quad \text{a.s.},$$

which leads to

$$\int_0^\infty e^{-rt}\Big(-(b+r)(\widehat{p}_t - p_t) + c_\bullet^\theta \cdot (\widehat{\gamma}_{\bullet,t} - \gamma_{\bullet,t})\Big)\mathrm{d}t = 0, \quad \text{a.s.},$$

owing to (12). Consequently, (10) rewrites as

$$\begin{aligned}
&J(\widehat{\gamma}_\bullet) - J(\gamma_\bullet)\\
&= \mathbb{E}\Bigg[\int_0^\infty e^{-rt}\Bigg(\frac{\mathrm{AP}}{r+b}c_\bullet^\theta \cdot (\widehat{\gamma}_{\bullet,t} - \gamma_{\bullet,t}) - \alpha_{\bullet,t}^\theta \cdot \big(\widehat{\gamma}_{\bullet,t} - \gamma_{\bullet,t}\big) - \beta_{\bullet,t}^\theta \cdot \big((\widehat{\gamma}^2)_{\bullet,t} - (\gamma^2)_{\bullet,t}\big)\\
&\qquad - \ell_1(\mathbf{1}\cdot\widehat{\gamma}_{\bullet,t} - \widetilde{\gamma}_t) + \ell_1(\mathbf{1}\cdot\gamma_{\bullet,t} - \widetilde{\gamma}_t) + \ell_2(\widetilde{\gamma}_t - \mathbf{1}\cdot\widehat{\gamma}_{\bullet,t}) - \ell_2(\widetilde{\gamma}_t - \mathbf{1}\cdot\gamma_{\bullet,t})\Bigg)\mathrm{d}t\Bigg]\\
&= \mathbb{E}\left[\int_0^\infty e^{-rt}\Big(f_t(\widehat{\gamma}_{\bullet,t}) - f_t(\gamma_{\bullet,t})\Big)\mathrm{d}t\right].
\end{aligned}$$

As $\widehat{\gamma}_{\bullet,t}$ maximizes $f_t(\cdot)$ for any t, we have proved the announced statement. Moreover, we can show that $t \mapsto \widehat{\gamma}_{\bullet,t}$ is measurable, see Appendix B for detail. □

Proof of Theorem 2. The strict concavity of $f_t^i(\cdot)$ on the convex set $\mathcal{G}_t^i$ ensures that the set of maximizers of $\widehat{\gamma}_{\bullet,t}^i$ is reduced to a singleton. □

Proof of Theorem 3. We omit the index i. In view of Theorem 2, it is enough to prove that for any t, the continuous function f_t is strictly concave with the current choice of loss functions $\ell_1 = \omega_1(x_+)^2$ and $\ell_2 = \omega_2(x_+)^2$. At any given t, the Hessian matrix is

$$\big(D^2 f_t(\gamma_\bullet)\big)_{\mathsf{e},\mathsf{e}'} := \frac{\partial^2 f_t(\gamma_\bullet)}{\partial\gamma_\mathsf{e}\,\partial\gamma_{\mathsf{e}'}} = -2\mathbf{1}_{\mathsf{e}=\mathsf{e}'}\beta_{\mathsf{e},t}^\theta - 2\omega_1\mathbf{1}_{E_t} + 2\omega_2\mathbf{1}_{E_t^c}, \qquad \mathsf{e},\mathsf{e}' \in \mathscr{E},$$

where $E_t := \{\widetilde{\gamma}_t < \mathbf{1}\cdot\gamma_\bullet\}$. On the set of $\gamma_\bullet$ such that E_t holds, then $D^2 f_t(\gamma_\bullet)$ is obviously negative definite because we have assumed $\beta_{\mathsf{e},t}^\theta > 0$ for any e and t, and $\omega_1 \ge 0$. On the complementary set where $\mathbf{1}_{E_t} = 0$, the sign analysis is less straightforward. Let us compute the associated quadratic form: for any non-zero $x_\bullet = (x_\mathsf{e})_{\mathsf{e}\in\mathscr{E}} \in \mathbb{R}^{|\mathscr{E}|}$, we have

$$\begin{aligned}
\frac{1}{2}x_\bullet \cdot D^2 f_t(\gamma_\bullet)x_\bullet &= -\sum_{\mathsf{e}\in\mathscr{E}}\beta_{\mathsf{e},t}^\theta x_\mathsf{e}^2 + \omega_2\Big(\sum_{\mathsf{e}\in\mathscr{E}} x_\mathsf{e}\Big)^2\\
&\le -\sum_{\mathsf{e}\in\mathscr{E}}\beta_{\mathsf{e},t}^\theta x_\mathsf{e}^2 + \omega_2\Big(\sum_{\mathsf{e}\in\mathscr{E}}\frac{1}{\beta_{\mathsf{e},t}^\theta}\Big)\Big(\sum_{\mathsf{e}\in\mathscr{E}}\beta_{\mathsf{e},t}^\theta x_\mathsf{e}^2\Big) < 0,
\end{aligned}$$

since $\omega_2\big(\sum_{\mathsf{e}\in\mathscr{E}}\frac{1}{\beta_{\mathsf{e},t}^\theta}\big) < 1$ and $\sum_{\mathsf{e}\in\mathscr{E}}\beta_{\mathsf{e},t}^\theta x_\mathsf{e}^2 > 0$. We have proved that, in any case, $D^2 f_t(\gamma_\bullet)$ is negative definite, i.e., f_t is strictly concave. □

2.5 An explicit example

We now offer efficient emission strategies with explicit formulas based on Example 1 and Theorem 3.

Theorem 4. *Assume that the assumptions of Theorem 3 are in force. For any $t \geq 0$, define*

$$\Gamma_t^i := \frac{\mathbf{1}}{2\beta_{\bullet,t}^{i,\theta}} \cdot \Big(\frac{\mathrm{AP}^i\, c_{\bullet}^{i,\theta}}{r+b^i} - \alpha_{\bullet,t}^{i,\theta}\Big), \qquad \xi_{1,t}^i := \omega_1^i \Big(\mathbf{1} \cdot \frac{1}{\beta_{\bullet,t}^{i,\theta}}\Big), \qquad \xi_{2,t}^i := \omega_2^i \Big(\mathbf{1} \cdot \frac{1}{\beta_{\bullet,t}^{i,\theta}}\Big)$$

and assume that for all $\mathsf{e} \in \mathscr{E}^i$,

$$0 < \frac{\mathrm{AP}^i\, c_{\mathsf{e}}^{i,\theta}}{r+b^i} - \alpha_{\mathsf{e},t}^{i,\theta} - \frac{2\omega_1^i}{1+\xi_{1,t}^i}\big(\Gamma_t^i - \widetilde{\gamma}_t^i\big)^+ - \frac{2\omega_2^i}{1-\xi_{2,t}^i}\big(\widetilde{\gamma}_t^i - \Gamma_t^i\big)^+ < 2\beta_{\mathsf{e},t}^{i,\theta}\lambda_{\mathsf{e},t}^{\max}. \tag{13}$$

Then, the optimal emission strategy for the energy source e has the explicit form

$$\widehat{\gamma}_{\mathsf{e},t}^i = \frac{1}{2\beta_{\mathsf{e},t}^{i,\theta}}\Big(\frac{\mathrm{AP}^i\, c_{\mathsf{e}}^{i,\theta}}{r+b^i} - \alpha_{\mathsf{e},t}^{i,\theta} - \frac{2\omega_1^i}{1+\xi_{1,t}^i}\big(\Gamma_t^i - \widetilde{\gamma}_t^i\big)^+ - \frac{2\omega_2^i}{1-\xi_{2,t}^i}\big(\widetilde{\gamma}_t^i - \Gamma_t^i\big)^+\Big). \tag{14}$$

Furthermore, the excess emission equals

$$\mathbf{1} \cdot \widehat{\gamma}_{\bullet,t}^i - \widetilde{\gamma}_t^i = \frac{1}{1+\xi_{1,t}^i}\big(\Gamma_t^i - \widetilde{\gamma}_t^i\big)^+ - \frac{1}{1-\xi_{2,t}^i}\big(\widetilde{\gamma}_t^i - \Gamma_t^i\big)^+. \tag{15}$$

Proof. We compute the gradient of (8). For any $t \geq 0$ and energy source $\mathsf{e} \in \mathscr{E}^i$,

$$\frac{\partial f_t^i}{\partial \gamma_{\mathsf{e},t}^i}(\gamma_{\bullet,t}^i) = \frac{\mathrm{AP}^i\, c_{\mathsf{e}}^{i,\theta}}{r+b^i} - \alpha_{\mathsf{e},t}^{i,\theta} - 2\beta_{\mathsf{e},t}^{i,\theta}\gamma_{\mathsf{e},t}^i - 2\omega_1^i\big(\mathbf{1}\cdot\gamma_{\bullet,t}^i - \widetilde{\gamma}_t^i\big)_+ - 2\omega_2^i\big(\widetilde{\gamma}_t^i - \mathbf{1}\cdot\gamma_{\bullet,t}^i\big)_+. \tag{16}$$

From Theorem 3, we know that f_t^i is strictly concave so that it is enough to check that $\widehat{\gamma}_{\mathsf{e},t}^i$ given by (14) is in $\big(0, \lambda_{\mathsf{e},t}^{\max}\big)$ (the interior of the constraint set) and cancels (16). The verification that $\widehat{\gamma}_{\mathsf{e},t}^i \in \big(0, \lambda_{\mathsf{e},t}^{\max}\big)$ is immediate from the condition (13).

Let us now verify that $\widehat{\gamma}_{\mathsf{e},t}^i$ cancels (16) and verifies (15). Consider the first case where $\Gamma_t^i \geq \widetilde{\gamma}_t^i$: summing over e in (14), we have

$$\begin{aligned}\mathbf{1}\cdot\widehat{\gamma}_{\bullet,t}^i - \widetilde{\gamma}_t^i &= \Gamma_t^i - \frac{\xi_{1,t}^i}{1+\xi_{1,t}^i}\big(\Gamma_t^i - \widetilde{\gamma}_t^i\big) - \widetilde{\gamma}_t^i \\ &= \frac{1}{1+\xi_{1,t}^i}\big(\Gamma_t^i - \widetilde{\gamma}_t^i\big),\end{aligned}$$

and therefore, we get

$$\begin{aligned}\frac{\partial f_t^i}{\partial \gamma_{\mathsf{e},t}^i}(\widehat{\gamma}_{\bullet,t}^i) &= \frac{\mathrm{AP}^i\, c_{\mathsf{e}}^{i,\theta}}{r+b^i} - \alpha_{\mathsf{e},t}^{i,\theta} - \Big(\frac{\mathrm{AP}^i\, c_{\mathsf{e}}^{i,\theta}}{r+b^i} - \alpha_{\mathsf{e},t}^{i,\theta} - \frac{2\omega_1^i}{1+\xi_{1,t}^i}\big(\Gamma_t^i - \widetilde{\gamma}_t^i\big)\Big) - \frac{2\omega_1^i}{1+\xi_{1,t}^i}\big(\Gamma_t^i - \widetilde{\gamma}_t^i\big) \\ &= 0.\end{aligned}$$

Consider now the second case where $\Gamma_t^i < \widetilde{\gamma}_t^i$. A similar computation gives

$$\begin{aligned}\widetilde{\gamma}_t^i - \mathbf{1}\cdot\widehat{\gamma}_{\bullet,t}^i &= \widetilde{\gamma}_t^i - \Gamma_t^i + \frac{\xi_{2,t}^i}{1-\xi_{2,t}^i}\big(\widetilde{\gamma}_t^i - \Gamma_t^i\big) \\ &= \frac{1}{1-\xi_{2,t}^i}\big(\widetilde{\gamma}_t^i - \Gamma_t^i\big)\end{aligned}$$

and consequently, it readily follows that

$$\frac{\partial f_t^i}{\partial \gamma_{\mathtt{e},t}^i}(\widehat{\gamma}_{\bullet,t}^i) = \frac{\mathrm{AP}^i\, c_{\mathtt{e}}^{i,\theta}}{r+b^i} - \alpha_{\mathtt{e},t}^{i,\theta} - \Big(\frac{\mathrm{AP}^i\, c_{\mathtt{e}}^{i,\theta}}{r+b^i} - \alpha_{\mathtt{e},t}^{i,\theta} - \frac{2\omega_2^i}{1-\xi_{2,t}^i}\big(\widetilde{\gamma}_t^i - \Gamma_t^i\big)\Big) - \frac{2\omega_2^i}{1-\xi_{2,t}^i}\big(\widetilde{\gamma}_t^i - \Gamma_t^i\big)$$
$$= 0.$$

The proof is complete. □

Remark 3. The interpretations of the above results are as follows. First, when there is no penalty or reward policy, then the obligor's optimal emission strategy for each energy $\mathtt{e}$ is

$$\frac{1}{2\beta_{\mathtt{e},t}^{i,\theta}}\Big(\frac{c_{\mathtt{e}}^{i,\theta}}{r+b^i} - \alpha_{\mathtt{e},t}^{i,\theta}\Big).$$

When the incentive policies are incorporated, that is, when ω_1 and ω_2 become strictly positive, the obligor reduces its emissions level. Second, the price of a given energy $\alpha_{\mathtt{e},t}^{i,\theta}$ is bounded from above by a certain level so that the energy $\mathtt{e}$ is chosen by the obligor. In the opposite case, the emission by the corresponding energy may drop to zero, meaning that the obligor prefers to avoid $\mathtt{e}$ and choose other types of energy.

3 Modeling the physical risk of each portfolio obligor

Now, we model the physical risk and its effect on the obligor's value process. Inspired by actuarial science, especially ruin theory [1], we model our aggregate loss as a compound Poisson process, capturing the randomness of physical risk events in time, independent inter-arrival intervals, and random losses denoted as Z. Our goal, however, is to provide a more tailored analysis specific to the obligor of interest. In our study, we incorporate the temporal evolution of the magnitude of physical risks, offering a detailed and dynamic perspective on how these risks affect the obligor.

3.1 Disintegrating the physical risk over climate and weather event types

In our modeling, we aim to consider two specific aspects:

1. Not all climate and weather events are relevant to a particular obligor.
2. The obligor's exposures vary based on the geographical zones of its offices and factories.

Climate extremes (droughts, heatwaves, sea level rise, etc) pertain to long-term, persistent deviations from typical climate conditions, while weather extreme events (tornadoes, blizzards, tsunamis, etc) are short-term, intense deviations from normal weather patterns. They both occur on different timescales (typically from hours to a few days for weather-extreme events) and have distinct characteristics. Types of climate extremes and weather extreme events $\mathtt{cw}$ are extensively detailed in [33] and consist of

$$\begin{aligned}\mathcal{CW} := \big\{&\text{storm/typhoon/hurricane/tornado/tropical cyclone,}\\ &\text{hailstorm, flood, winter storm, level sea rise, and storm surge,}\\ &\text{heat wave, drought, wildfire, extreme cold spells, snowstorms, and blizzards,}\ldots\big\}.\end{aligned}$$

For each climate and weather event $\mathtt{cw}$ and geographical zone l, we associate a Poisson process $N^{\mathtt{cw},l}$ (defined on the same filtered probability space as before) with a deterministic intensity $t \mapsto \lambda_t^{\mathtt{cw},l}$. The intensity varies over time due to the global impact of climate change, which increases the frequency of extreme weather events. However, the outcome is location-dependent, with some areas experiencing heightened frequencies while others may see decreases. We refer

to [17] for the mathematical definition of a time-inhomogeneous Poisson process. While these Poisson processes could be defined with interdependencies, they do not affect the subsequent derivation, as we demonstrate.

When a climate and weather event $\texttt{cw}$ occurs in a geographical zone l and time u, the ith obligor experiences an immediate loss $Z_u^{i,\texttt{cw},l}$ [6] resulting from the obligor's vulnerability and exposure to climate events. Over a time interval $[t_0, t_1]$, the cumulative loss incurred by the ith obligor is

$$\int_{t_0}^{t_1} \sum_{\texttt{cw},l} Z_u^{i,\texttt{cw},l} \, \mathrm{d}N_u^{\texttt{cw},l}.$$

3.2 Expected damage for an obligor

The obligor is making provisions for these physical risks by discounting future losses with an interest rate r. This leads to the following definition of the Expected Physical Damage (EPD) as follows:

$$\mathrm{EPD}^i(t) := \mathbb{E}\Big[\sum_{\texttt{cw},l} \int_t^\infty e^{-r(u-t)} Z_u^{i,\texttt{cw},l} \mathrm{d}N_u^{\texttt{cw},l} \Big| \mathcal{F}_t\Big]. \tag{17}$$

From the properties of the compound process, we have

$$\mathrm{EPD}^i(t) = \int_t^\infty e^{-r(u-t)} \Big(\sum_{\texttt{cw},l} \mathbb{E}\big[Z_u^{i,\texttt{cw},l}\big] \, \lambda_u^{\texttt{cw},l} \Big) \mathrm{d}u.$$

It is worth noting that neither the dependence between Poisson processes nor the relationship between N and Z affects this representation.

3.3 Calibration procedure

To use the above description, we have to model the time evolution of

$$u \mapsto \mathbb{E}\big[Z_u^{i,\texttt{cw},l}\big], \qquad u \mapsto \lambda_u^{\texttt{cw},l},$$

according to each geographical zone l and climate and weather event $\texttt{cw}$.

Empirical studies, like [16], reveal a strong connection between the frequencies $\lambda_u^{\texttt{cw},l}$ of climate events, mean losses $\mathbb{E}\big[Z_u^{i,\texttt{cw},l}\big]$, and the climate mitigation trajectory linked to a specific SSP. In a scenario like SSP5, characterized by significant warming, obligors would face more frequent and substantial losses. Conversely, in a greener, highly mitigated scenario like SSP1, losses would be far less frequent and severe. We suggest a simplified, realistic model suitable for straightforward calibration.

From the Nordhaus model [26, 25] (also known as the DICE model – Dynamic Integrated model of Climate and the Economy), we know that $\mathbb{E}\big[Z_u^{i,\texttt{cw},l}\big]$ and $\lambda_u^{\texttt{cw},l}$ depend on the global rise in atmospheric temperature $\mathcal{T}_{\mathrm{ATM}}$ through a damage function $\mathcal{D}$. In the initial DICE model, the damage is quadratic:

$$\mathcal{D}\big(\mathcal{T}_{\mathrm{ATM}}\big) = a_1 \mathcal{T}_{\mathrm{ATM}} + a_2 \mathcal{T}_{\mathrm{ATM}}^2 \tag{18}$$

with $a_1 = 0$, $a_2 = 0.0028388$ (2008 version of DICE). Alternative functions have been proposed in the literature; see [35, 14], for instance. Note that $\mathcal{T}_{\mathrm{ATM}}$ refers to the global average temperature increase relative to the pre-industrial era. For simplicity, we assume the damage function is identical for all companies and independent of $\texttt{cw}$ and l.

We assume that $\sum_{\texttt{cw},l} \mathbb{E}\big[Z_u^{i,\texttt{cw},l}\big] \, \lambda_u^{\texttt{cw},l}$ evolves proportionally to $\mathcal{D}(\mathcal{T}_{\mathrm{ATM}}(u))$, where the path of the atmosphere temperature is given by the selected SSP and denoted $u \to \mathcal{T}_{\mathrm{ATM}}(u)$, see

[6] on the mathematical side, $Z^{i,\texttt{cw},l}$ is a càglàd process

Figure 5 for some relative temperature paths for different SSP scenarios. All in all, our model of physical damages for the ith obligor becomes

$$\mathrm{EPD}^i(t) := \Big(\sum_{\mathtt{cw},l} \mathbb{E}\big[Z^{i,\mathtt{cw},l}_{t_{\mathrm{ref}}}\big]\lambda^{\mathtt{cw},l}_{t_{\mathrm{ref}}}\Big)\int_t^\infty e^{-r(u-t)}\frac{\mathcal{D}(\mathcal{T}_{\mathrm{ATM}}(u))}{\mathcal{D}(\mathcal{T}_{\mathrm{ATM}}(t_{\mathrm{ref}}))}\mathrm{d}u, \tag{19}$$

where t_{ref} is the time at which the model is calibrated.

Calculating the total physical losses of the obligor $\Big(\sum_{\mathtt{cw},l} \mathbb{E}\big[Z^{i,\mathtt{cw},l}_{t_{\mathrm{ref}}}\big]\lambda^{\mathtt{cw},l}_{t_{\mathrm{ref}}}\Big)$ is based on historical obligor data. Note that we are not accounting for any changes the obligor may have made to its operations or locations in recent years. Observe also that the integral factor is common across all companies. In essence, when evaluating future physical risk, we begin with historical losses and apply a scenario-dependent multiplicative factor

$$\int_t^\infty e^{-r(u-t)}\frac{\mathcal{D}(\mathcal{T}_{\mathrm{ATM}}(u))}{\mathcal{D}(\mathcal{T}_{\mathrm{ATM}}(t_{\mathrm{ref}}))}\mathrm{d}u.$$

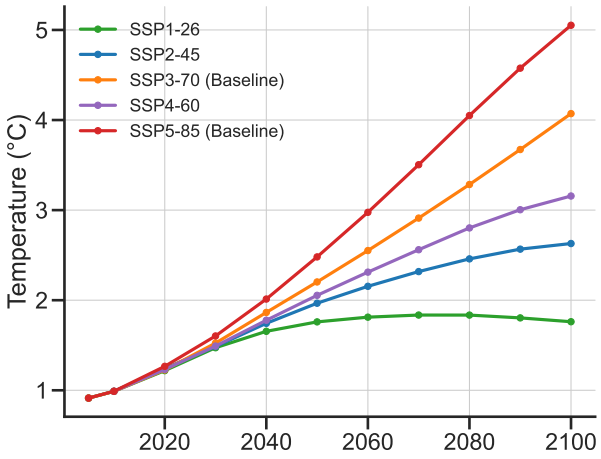

Figure 5: Global average temperature increase relative to the pre-industrial era (year 1750) for different SSPs. Source: [29], https://ourworldindata.org/.

4 Obligor's default probability in an explicit model

We model the default event as in the structural credit approach, [31, Chapter 3]. At a given time $t \geq 0$, an obligor defaults if its value is inferior to its debt and liability level. The probability of default for the ith obligor is

$$\mathrm{PD}^i_t = \mathbb{P}\left(\widehat{V}^i_t \leq L^i(t)\right)$$

where the obligor's value $\widehat{V}^i_t$ is impacted by both transition and physical risks, and the default barrier $L^i(t)$ is a deterministic function which represents the minimal level of the obligor's liability payment such as the debt reimbursement and the labor cost of the obligor at time t.

In the following, we define the obligor's value $\widehat{V}^i_t$ as the conditional discounted value of the obligor's future cashflow at time $t \geq 0$ with the optimal emission strategy $\widehat{\gamma}^i$, minus the expected physical damages (17). We also take losses functions $\ell_1(\cdot), \ell_2(\cdot)$ to be the same as in Example 1.

This yields

$$\begin{aligned}\widehat{V}_t^i := \mathbb{E}\Bigg[\int_t^\infty e^{-r(u-t)}\Big(&\mathrm{AP}^i \times \widehat{P}_u^i - \alpha^{i,\theta}_{\bullet,u}\cdot\widehat{\gamma}^i_{\bullet,u} - \beta^{i,\theta}_{\bullet,u}\cdot(\widehat{\gamma}^2)^i_{\bullet,u}\\ &- \omega_1^i\left(\mathbf{1}\cdot\widehat{\gamma}^i_{\bullet,u} - \widetilde{\gamma}^i_u\right)_+^2 + \omega_2^i\left(\widetilde{\gamma}^i_u - \mathbf{1}\cdot\widehat{\gamma}^i_{\bullet,u}\right)_+^2\Big)\mathrm{d}u\,\Big|\,\mathcal{F}_t\Bigg]\\ &- \mathrm{EPD}^i(t),\end{aligned} \tag{20}$$

where $\widehat{P}^i$ denotes the optimal production associated with $\widehat{\gamma}^i_\bullet$. We note that although the optimization is conducted with the logarithmic function, we here use the total production for the computation of the obligor's value.

Recall that in the explicit model of Section 2.5, the optimal emission $\widehat{\gamma}^i_\bullet$ is deterministic and explicitly given by (14). When the benchmark $\widetilde{\gamma}^i$ is low (strict mitigation scenario), the penalty coefficient ω_1^i plays an essential role in the optimal strategy, while for a relatively loose scenario when the benchmark is high, the reward coefficient ω_2^i is more important.

To facilitate the subsequent aggregation of losses across different obligors, let us first describe the stochastic distribution of log production. From (2) and (3), the optimal log production $\widehat{p}^i$ is

$$\begin{aligned}\widehat{p}^i_u = e^{-b^i(u-t)}\widehat{p}^i_t + \frac{a^i}{b^i}(1-e^{-b^i(u-t)}) + \int_t^u e^{-b^i(u-s)}(c^{i,\theta}_\bullet\cdot\widehat{\gamma}^i_{\bullet,s})\mathrm{d}s\\ + \sigma^i\int_t^u e^{-b^i(u-s)}\left(\rho^i\mathrm{d}B_s + \sqrt{1-(\rho^i)^2}\,\mathrm{d}B^i_s\right),\end{aligned} \tag{21}$$

for all $u \geq t$.

Conditionally on $\mathcal{F}_t$, $\left(\widehat{p}^i_u\right)_{1\leq i\leq n}$ is an n-dimensional Gaussian vector with conditional mean

$$\begin{aligned}\mathbb{E}\left[\widehat{p}^i_u|\mathcal{F}_t\right] &= e^{-b^i(u-t)}\widehat{p}^i_t + \frac{a^i}{b^i}(1-e^{-b^i(u-t)}) + \int_t^u e^{-b^i(u-s)}(c^{i,\theta}_\bullet\cdot\widehat{\gamma}^i_{\bullet,s})\,\mathrm{d}s\\ &=: e^{-b^i(u-t)}\widehat{p}^i_t + m^i(u,t),\end{aligned} \tag{22}$$

and conditional covariance

$$\mathrm{Cov}\left(\widehat{p}^i_u,\widehat{p}^j_u|\mathcal{F}_t\right) := \Sigma^{i,j}(u-t) = \sigma^i\sigma^j\left(\rho^i\rho^j\mathbf{1}_{i\neq j} + \mathbf{1}_{i=j}\right)\frac{1-e^{-(b^i+b^j)(u-t)}}{b^i+b^j}, \tag{23}$$

for every $i,j\in\{1,\ldots,n\}$.

5 Aggregated loss distribution of the portfolio

5.1 Modeling the loss

In this section, we consider the loss portfolio and its computation. Let the loss portfolio be defined as

$$\mathcal{L}_t = \sum_{i=1}^n \Lambda^i \times \mathbf{1}_{\left\{\widehat{V}^i_t \leq L^i(t)\right\}} \tag{24}$$

where $\Lambda^i = \mathrm{EAD}^i \times \mathrm{LGD}^i$ and $\mathrm{LGD}^i, \mathrm{EAD}^i$ are respectively the loss given default and exposure at default associated with the ith obligor. The time horizon t is typically chosen to be one year according to the solvency regulation. If interested in longer-time horizons, conditional losses can also be considered as our problem setting is Markovian.

From (19), (20), and the fact that $\mathbb{E}\big[\widehat{P}^i_u|\mathcal{F}_t\big] = \exp\big(e^{-b^i(u-t)}\widehat{p}^i_t + m^i(u,t) + \frac{1}{2}\Sigma^{i,i}(u-t)\big)$, we have

$$\widehat{V}^i_t = h^i\big(t, \widehat{p}^i_t\big)$$

where the deterministic function $h^i(\cdot,\cdot)$ is defined for all $t \geq 0$ and $x \in \mathbb{R}$ as

$$\begin{aligned} h^i(t,x) := \mathrm{AP}^i \int_t^\infty e^{-r(u-t)} \exp\Big(e^{-b^i(u-t)}x + m^i(u,t) + \frac{1}{2}\Sigma^{i,i}(u-t)\Big)\,\mathrm{d}u \\ - \int_t^\infty e^{-r(u-t)}\Big(\alpha^{i,\theta}_{\bullet,u}\cdot\widehat{\gamma}^i_{\bullet,u} + \beta^{i,\theta}_{\bullet,u}\cdot(\widehat{\gamma}^2)^i_{\bullet,u} + \omega^i_1\big(\mathbf{1}\cdot\widehat{\gamma}^i_{\bullet,u} - \widetilde{\gamma}^i_u\big)^2_+ - \omega^i_2\big(\widetilde{\gamma}^i_u - \mathbf{1}\cdot\widehat{\gamma}^i_{\bullet,u}\big)^2_+\Big)\,\mathrm{d}u \\ - \mathrm{EPD}^i(t). \end{aligned} \tag{25}$$

Note that $h^i(t,\cdot)$ is a continuous increasing bijection from $\mathbb{R}$ to $(0,+\infty)$, for any t.

The portfolio loss rewrites as

$$\begin{aligned} \mathcal{L}_t &= \sum_{i=1}^n \Lambda^i\,\mathbf{1}_{\left\{h^i(t,\widehat{p}^i_t)\leq L^i(t)\right\}} \\ &= \sum_{i=1}^n \Lambda^i\,\mathbf{1}_{\left\{\widehat{p}^i_t\leq (h^i(t,\cdot))^{-1}(L^i(t))\right\}} \\ &= \sum_{i=1}^n \Lambda^i\,\mathbf{1}_{\left\{e^{-b^it}\widehat{p}^i_0 + m^i(t,0) + \sigma^i\sqrt{1-(\rho^i)^2}\int_0^t e^{-b^i(t-s)}\,\mathrm{d}B^i_s - (h^i(t,\cdot))^{-1}(L^i(t))\leq -\sigma^i\rho^i\int_0^t e^{-b^i(t-s)}\,\mathrm{d}B_s\right\}} \\ &= \sum_{i=1}^n \Lambda^i\,\mathbf{1}_{\left\{A^i_t\leq X^i_t\right\}} \end{aligned}$$

$$\text{with}\quad A^i_t := \frac{1}{\sigma^i}\left[e^{-b^it}\,\widehat{p}^i_0 + m^i(t,0) + \sigma^i\sqrt{1-(\rho^i)^2}\int_0^t e^{-b^i(t-s)}\,\mathrm{d}B^i_s - (h^i(t,\cdot))^{-1}(L^i(t))\right],$$

$$X^i_t := -\rho^i\int_0^t e^{-b^i(t-s)}\,\mathrm{d}B_s.$$

Analyzing the distribution of $\mathcal{L}_t$ is intricate. Analytical methods are not suitable due to it being a weighted sum of correlated Bernoulli random variables with varying dependencies. An alternative Monte Carlo simulation is feasible but time-consuming for several reasons: a) in typical cases, there are many obligors (n is large); b) the number of correlated Gaussian random variables is large (as large as n) making sampling $\mathcal{L}_t$ costly; c) numerous $\mathcal{L}_t$ samples are required, especially for tail event risk management.

To tackle these challenges, we utilize two efficient dimension reduction methods, leveraging multiple enhancements.

- The distribution of the vector $X_t = (X^i_t)_{1\leq i\leq n}$ is Gaussian. An initial, naive assumption might be that the rank of its covariance matrix K_{X_t} approximately equals the number of distinct b^i, and that all eigenvalues hold significant importance. However, this intuition is considerably flawed. A thorough examination of the spectral decomposition of K_{X_t} reveals a surprising result: the top two eigenvalues account for over 99% of the total variance (i.e., the trace of K_{X_t}). Consequently, we first perform a Principal Component Analysis (PCA) on the vector X_t, reducing it to two principal factors. For an in-depth analysis, refer to Section 5.2.

- This approach allows us to express the loss $\mathcal{L}_t$ as a sum of indicator functions with n independent Gaussian random variables (for $\int_0^t e^{-b^i(t-s)}\mathrm{d}B^i_s$) and two common factors derived from the PCA. Utilizing a two-dimensional Polynomial Chaos Expansion (PCE) for indicator functions as outlined in [6], and retaining the first M terms (typically $M = 6$ or 10 suffices), we further approximate $\mathcal{L}_t$ using a multivariate Gaussian random variable with

a dimension of $M+2$ and involving a summation of M^2 terms, instead of $2n$ Gaussian random variables and n terms in the sum. Recall that typically $n \approx 10^6$ for major banks: in comparison with the new cost $M^2 \lessapprox 100$, the improvement in complexity is huge. This is elaborated in Subsection 5.3.

In summary, this significantly reduces the overall computational cost of our climate credit model.

5.2 Principal Component Analysis (PCA) of $X_t := (X_t^i)_{1\le i\le n}$

Let $K_{X_t} = \left((K_{X_t})^{i,j}\right)_{1\le i,j\le n}$ be the covariance matrix of X_t. We have

$$(K_{X_t})^{i,j} := \mathrm{Cov}(X_t^i, X_t^j) = \rho^i\rho^j \int_0^t e^{-b^i(t-s)}e^{-b^j(t-s)}\mathrm{d}s = \rho^i\rho^j \frac{1-e^{-(b^i+b^j)t}}{b^i+b^j}. \tag{26}$$

Following [10, Section 3.2], the spectral decomposition of K_{X_t} writes as

$$K_{X_t} = \sum_{k=1}^n \nu^k u^k (u^k)^\top$$

where $(\nu^k)_{1\le k\le n}$ are the eigenvalues (in decreasing order) and $(u^k)_{1\le k\le n}$ are the eigenvectors of K_{X_t}. Since the latter is a positive semi-definite matrix, $\nu^k \ge 0$ for all k. Equivalently,

$$X_t = \sum_{k=1}^n \sqrt{\nu^k} G^k u^k \tag{27}$$

where the $(G^k)_{1\le k\le n}$ are independent $\mathcal{N}(0,1)$ random variables.

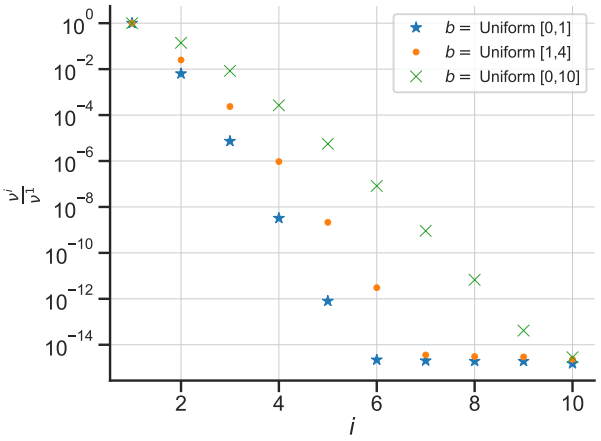

Figure 6: Ratio $\frac{\nu^k}{\nu^1}$ for k from 1 to 10 with $n = 1000$, $\rho \sim \mathcal{U}[-1,1]$ and $b \sim \mathcal{U}[0,1]$, $\mathcal{U}[1,4]$, and $\mathcal{U}[0,10]$.

Note that when the b^i are constant (say equal to $b > 0$), we can write $K_{X_t} = \boldsymbol{\rho}\boldsymbol{\rho}^\top \frac{1-e^{-2bt}}{2b}$ (where $\boldsymbol{\rho}$ is the vector of ρ^i) and therefore, the rank of K_{X_t} equals 1 at most ($\nu^k = 0$ for $k = 2, \cdots n$). For non-constant b, we observe (see Figures 6 and 7) that K_{X_t} generally resembles a low-rank symmetric matrix, where only the first two eigenvalues ν^1 and ν^2 matter. This can be assessed using the inertia:

$$\frac{\sum_{k=1}^2 \nu^k}{\sum_{k=1}^n \nu^k}.$$

The above depends on b^i and n and in our experiments, it is very close to 1. namely, we take $\rho^i \sim \mathcal{U}[-1,1]$ and three distinct cases for the b^i:

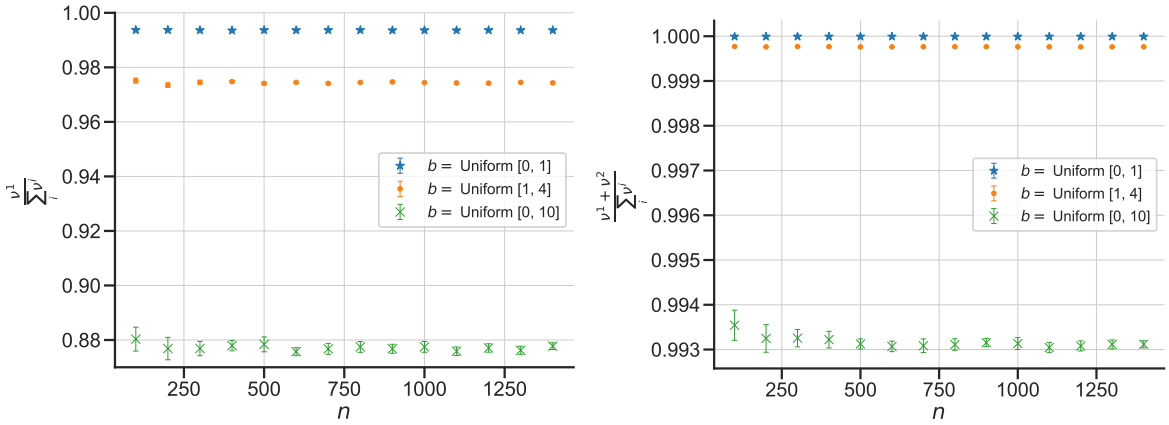

Figure 7: Ratio $\frac{\nu^1}{\sum_{k=1}^n \nu^k}$ (left) and $\frac{\nu^1+\nu^2}{\sum_{k=1}^n \nu^k}$ (right) for n from 100 to 1500, $\rho \sim \mathcal{U}[-1,1]$ and $b \sim \mathcal{U}[0,1]$, $\mathcal{U}[1,4]$, and $\mathcal{U}[0,10]$. For each ratio, we provide the 95% confidence interval with 30 independent runs.

- $b^i \sim \mathcal{U}[0,1]$: the rank of K_{X_t} is very close to one, corresponding to the scenario where b is nearly constant.
- $b^i \sim \mathcal{U}[1,4]$: this is the typical case in practice, the characteristic time $1/b$ falls between one quarter and one year.
- $b^i \sim \mathcal{U}[0,10]$: to illustrate that a rank-two approximation remains acceptable even as the variance increases.

In Figure 6, we plot the ratio ν^k/ν^1 from $k=1$ to 10 with $n=1000$ for a single realization of ρ^i and b^i. The plot demonstrates that the ratio decreases extremely rapidly. Specifically, when $b^i \sim \mathcal{U}[0,10]$, the ratio $\nu^3/\nu^1 \approx 10^{-2}$, and it is close to 10^{-5} when $b^i \sim \mathcal{U}[0,1]$. In Figure 7, we plot $\frac{\nu^1}{\sum_k \nu^k}, \frac{\nu^1+\nu^2}{\sum_k \nu^k}$, using boxplots over 100 replications for n ranging from 100 to 1500. The results show that the two eigenvalues account for 99% of the total variance when $b^i \sim \mathcal{U}[0,10]$, and 99.99% otherwise. We have not yet been able to precisely quantify this property theoretically, including the selection of the reduced dimension. Furthermore, to the best of our knowledge, this phenomenon has not been documented in the existing literature on random matrices.

We now leverage these experimental observations to approximate the distribution of X_t with a low-dimensional Gaussian distribution. We choose to truncate (27) and keep only 2 terms:

$$X_t \approx \sum_{k=1}^{2} \sqrt{\nu^k} G^k u^k. \tag{28}$$

Denoting the coordinates of the two eigenvectors u^1, u^2 by $u^{1,i}, u^{2,i}$ for $i = 1, \dots, n$, the above expansion leads to an approximate model

$$\mathcal{L}_t \approx \mathcal{L}_t^{\mathrm{PCA}} := \sum_{i=1}^{n} \Lambda^i \mathbf{1}_{\left\{A_t^i \le \sqrt{\nu^1} G^1 u^{1,i} + \sqrt{\nu^2} G^2 u^{2,i}\right\}}. \tag{29}$$

Proposition 5. *The L_1 error between the original and approximated loss is bounded as follows:*

$$\mathbb{E}\left[\left|\mathcal{L}_t - \mathcal{L}_t^{\mathrm{PCA}}\right|\right] \le \sum_{i=1}^{n} \frac{\Lambda^i}{\pi} \frac{|\rho^i|}{\sqrt{1-(\rho^i)^2}} \sqrt{\frac{\sum_{k=3}^n \nu^k (u^{k,i})^2}{\sum_{k=1}^n \nu^k (u^{k,i})^2}}. \tag{30}$$

The smaller the eigenvalues $(\nu^k, k \ge 3)$ compared to the others, the better the approximation. We have focused on the PCA approximation, but we do not claim that the dependence of

constants is optimal with respect to the probabilistic characteristics of A_t^i. In particular, the estimate (30) does not account for the fact that we compute tail risks (the indicator functions in (24) are likely equal to 0, which is not reflected on the right-hand side of (30)).

Proof. A direct triangular inequality yields

$$\mathbb{E}\left[\left|\mathcal{L}_t - \mathcal{L}_t^{\mathrm{PCA}}\right|\right] \leq \sum_{i=1}^{n} \Lambda^i \, \mathbb{E}\left[\left|\mathbf{1}_{\left\{A_t^i \leq X_t^i\right\}} - \mathbf{1}_{\left\{A_t^i \leq \sqrt{\nu^1} G^1 u^{1,i} + \sqrt{\nu^2} G^2 u^{2,i}\right\}}\right|\right]. \tag{31}$$

To bound the above, we use bounds on the distribution of A_t^i. Recall that A_t^i has a Gaussian distribution with variance $(1-(\rho^i)^2)\frac{1-e^{-2b^i t}}{2b^i}$. Observe that we have the identity

$$(\rho^i)^2 \frac{1-e^{-2b^i t}}{2b^i} = \sum_{k=1}^{n} \nu^k (u^{k,i})^2;$$

this follows from the comparison of (26) and (27). Hence, the Gaussian density of A_t^i is uniformly bounded by

$$\frac{1}{\sqrt{2\pi}\sqrt{\sum_{k\geq 1} \nu^k (u^{k,i})^2}} \frac{|\rho^i|}{\sqrt{1-(\rho^i)^2}}.$$

If $X_t^i > \sqrt{\nu^1} G^1 u^{1,i} + \sqrt{\nu^2} G^2 u^{2,i}$, the difference of indicator functions in the right-hand side of (31) equals $\mathbf{1}_{\left\{\sqrt{\nu^1} G^1 u^{1,i} + \sqrt{\nu^2} G^2 u^{2,i} < A_t^i \leq X_t^i\right\}}$; in the other case, it is equal to $-\mathbf{1}_{\left\{X_t^i < A_t^i \leq \sqrt{\nu^1} G^1 u^{1,i} + \sqrt{\nu^2} G^2 u^{2,i}\right\}}$. Since A_t^i is independent of X_t^i and $\sqrt{\nu^1} G^1 u^{1,i} + \sqrt{\nu^2} G^2 u^{2,i}$, we get

$$\begin{aligned}
&\mathbb{E}\left[\left|\mathbf{1}_{\left\{A_t^i \leq X_t^i\right\}} - \mathbf{1}_{\left\{A_t^i \leq \sqrt{\nu^1} G^1 u^{1,i} + \sqrt{\nu^2} G^2 u^{2,i}\right\}}\right|\right] \\
&\leq \frac{1}{\sqrt{2\pi}\sqrt{\sum_{k=1}^{n} \nu^k (u^{k,i})^2}} \frac{|\rho^i|}{\sqrt{1-(\rho^i)^2}} \mathbb{E}\left[\left|X_t^i - \sqrt{\nu^1} G^1 u^{1,i} + \sqrt{\nu^2} G^2 u^{2,i}\right|\right]
\end{aligned}$$

The quantity inside in the absolute value is Gaussian distributed with mean zero and variance

$$\sum_{k=3}^{n} \nu^k (u^{k,i})^2.$$

In addition, we have $\mathbb{E}\left[|G^1|\right] = \sqrt{\frac{2}{\pi}}$. All in all, we obtain

$$\mathbb{E}\left[\left|\mathbf{1}_{\left\{A_t^i \leq X_t^i\right\}} - \mathbf{1}_{\left\{A_t^i \leq \sqrt{\nu^1} G^1 u^{1,i} + \sqrt{\nu^2} G^2 u^{2,i}\right\}}\right|\right] \leq \frac{1}{\pi} \frac{|\rho^i|}{\sqrt{1-(\rho^i)^2}} \sqrt{\frac{\sum_{k=3}^{n} \nu^k (u^{k,i})^2}{\sum_{k=1}^{n} \nu^k (u^{k,i})^2}}.$$

Plugging this into (31) readily completes the proof. □

5.3 Polynomial chaos expansion (PCE)

We further approximate $\mathcal{L}^{\mathrm{PCA}}$ using a polynomial chaos expansion (PCE). Write

$$\begin{aligned}
\mathcal{L}_t^{\mathrm{PCA}} &= \sum_{i=1}^{n} \Lambda^i \, \mathbf{1}_{\left\{\frac{A_t^i}{\sqrt{\nu^1 (u^{1,i})^2 + \nu^2 (u^{2,i})^2}} \leq \frac{\sqrt{\nu^1} u^{1,i} G^1 + \sqrt{\nu^2} u^{2,i} G^2}{\sqrt{\nu^1 (u^{1,i})^2 + \nu^2 (u^{2,i})^2}}\right\}} \\
&=: \sum_{i=1}^{n} \Lambda^i \, \mathbf{1}_{\left\{\tilde{A}_t^i \leq L^{1,i} G^1 + L^{2,i} G^2\right\}}
\end{aligned}$$

with $L^{k,i} := \frac{\sqrt{\nu^k} u^{k,i}}{\sqrt{\nu^1 (u^{1,i})^2 + \nu^2 (u^{2,i})^2}}$ for $k = 1, 2$ so that $(L^{1,i})^2 + (L^{2,i})^2 = 1$ and $\tilde{A}_t^i := \frac{A_t^i}{\sqrt{\nu^1 (u^{1,i})^2 + \nu^2 (u^{2,i})^2}}$. Observing that $L^{1,i} G^1 + L^{2,i} G^2 \sim \mathcal{N}(0,1)$, we apply a PCE of the indicator function at order M (see Proposition 8) to get

$$\begin{aligned}
\mathcal{L}_t^{\mathrm{PCA,PCE}} &:= \sum_{i=1}^{n} \Lambda^i \sum_{m=0}^{M} \tau_m(\tilde{A}_t^i)\, \mathrm{He}_m(L^{1,i} G^1 + L^{2,i} G^2) \\
&= \sum_{i=1}^{n} \Lambda^i \sum_{m=0}^{M} \tau_m(\tilde{A}_t^i) \sum_{\substack{m_1, m_2 \geq 0 \\ m_1 + m_2 = m}} \frac{m!}{m_1! m_2!} (L^{1,i})^{m_1} (L^{2,i})^{m_2} \mathrm{He}_{m_1}(G^1) \mathrm{He}_{m_2}(G^2)
\end{aligned}$$

where we have used [6, Lemma 3.5] at the second equality. Introducing the new random variables

$$\varepsilon_{n,m_1,m_2} := \sum_{i=1}^{n} \Lambda^i \, \tau_{m_1+m_2}(\tilde{A}_t^i) \frac{(m_1+m_2)!}{m_1! m_2!} (L^{1,i})^{m_1} (L^{2,i})^{m_2},$$

the approximate portfolio loss rewrites as

$$\mathcal{L}_t^{\mathrm{PCA,PCE}} = \sum_{m=0}^{M} \sum_{\substack{m_1, m_2 \geq 0 \\ m_1 + m_2 = m}} \varepsilon_{n,m_1,m_2} \mathrm{He}_{m_1}(G^1) \mathrm{He}_{m_2}(G^2). \tag{32}$$

In the approximation of large n, the ε_{n,m_1,m_2} being sums of independent random variables, we can approximate the $\frac{1}{2}(M+2)(M+1)$-dimensional vector $\left(\varepsilon_{n,m_1,m_2}\right)_{m_1+m_2=m,\, 0 \leq m \leq M}$ with a Gaussian vector $(\varepsilon^{\mathrm{G}}_{n,m_1,m_2})$ with mean vector $\mathcal{M}$ and covariance matrix $\mathcal{K}$ where for every $0 \leq m_1, m_1', m_2, m_2' \leq M$, we have

$$\begin{aligned}
\mathcal{M}_{m_1,m_2} &:= \mathbb{E}\left[\varepsilon_{n,m_1,m_2}\right] = \sum_{i=1}^{n} \Lambda^i \, \mathbb{E}\left[\tau_{m_1+m_2}\left(\tilde{A}_t^i\right)\right] \frac{(m_1+m_2)!}{m_1!\, m_2!} (L^{1,i})^{m_1} (L^{2,i})^{m_2}, \\
\mathcal{K}_{(m_1,m_2),(m_1',m_2')} &:= \mathrm{Cov}\left(\varepsilon_{n,m_1,m_2}, \varepsilon_{n,m_1',m_2'}\right) \\
&= \sum_{i=1}^{n} (\Lambda^i)^2 \, \mathrm{Cov}\left(\tau_{m_1+m_2}\left(\tilde{A}_t^i\right), \tau_{m_1'+m_2'}\left(\tilde{A}_t^i\right)\right) \\
&\quad \times \frac{(m_1+m_2)!}{m_1!\, m_2!} (L^{1,i})^{m_1} (L^{2,i})^{m_2} \frac{(m_1'+m_2')!}{m_1'!\, m_2'!} (L^{1,i})^{m_1'} (L^{2,i})^{m_2'},
\end{aligned} \tag{33}$$

taking advantage of the independence of $(\tilde{A}_t^i)_{1 \leq i \leq n}$. Our PCA-PCE portfolio loss with Gaussian approximation finally writes as

$$\mathcal{L}_t^{\mathrm{PCA,PCE,G}} := \sum_{m=0}^{M} \sum_{\substack{m_1, m_2 \geq 0 \\ m_1 + m_2 = m}} \varepsilon^{\mathrm{G}}_{n,m_1,m_2} \mathrm{He}_{m_1}(G^1) \mathrm{He}_{m_2}(G^2).$$

The parameters $\mathcal{M}, \mathcal{K}$ can be efficiently computed thanks to recursive relations, see Proposition 9 for details. The L_2 error due to the truncation between $\mathcal{L}^{\mathrm{PCA}}$ and $\mathcal{L}^{\mathrm{PCA,PCE}}$ is of order $(\sum_{i=1}^{n} \Lambda^i) M^{-\frac{1}{4}}$. Refined estimates for the L_2 error are available in [7, Theorem 2.7].

5.4 Numerical experiments

In this section, we aim to evaluate our methodology, focusing specifically on two key aspects: the improvement in computational speed and the performance of the PCA-PCE-based approximation. Additionally, we seek to assess the impact of physical risk on the portfolio loss.

We focus on three distinct SSP scenarios: SSP1-26, SSP3-70 (Baseline), and SSP5-85 (Baseline) for the transportation sector, see Figure 4. The portfolio loss maturity is set at $t = 5$ years, where $t = 0$ corresponds to 2015. We take $n_{\mathrm{mc}} = 10^5$ Monte Carlo samples for our analysis. We study the fictitious portfolio $\mathcal{A}$ with parameters:

Portfolio $\mathcal{A}$: $t = 5$ years, $n = 1,000$, $r = 2\%$, 3 different energy sources for $\mathtt{e}$, $c^i_{\mathtt{e}} = (0.01, 0.01, 0.01)$, $\omega_1 = 0.05$, $\omega_2 = 0.02$, $\alpha^i_{\bullet,t} = (0,0,0)$, $\beta^i_{\bullet,t} = (0.1, 0.5, 0.8)$, $\theta^i_{\bullet,t} = (1,1,1)$, $P_0 = 1$, $\sigma^i \overset{\text{i.i.d.}}{\sim} \mathcal{U}[0, \frac{1}{2}]$, $a^i \overset{\text{i.i.d.}}{\sim} \mathcal{U}[0, \frac{1}{2}]$, $b^i \overset{\text{i.i.d.}}{\sim} \mathcal{U}[1,4]$, $\rho^i \overset{\text{i.i.d.}}{\sim} \mathcal{U}[-1,1]$, $\Lambda^i = \frac{1}{\sqrt{i}}$, $\mathrm{AP}^i = 1$, $\lambda_{\text{ref}} = 3\%$.

5.4.1 Physical Risk Impact

In light of Section 3, to account for the physical risk associated with the portfolio, we must compute the expected physical damage EPD^i for each obligor i. From (20), we observe that when accounting for physical risk, the default barrier $L^i(t)$ increases by the amount EPD^i.

To compute EPD^i as described in (19), we assume that the sum of the total physical losses amounts to 0.001% of the obligor's current value. This is represented by $\sum_{\mathtt{cw},l} \mathbb{E}\big[Z^{i,\mathtt{cw},l}_{t_{\text{ref}}}\big] \lambda^{\mathtt{cw},l}_{t_{\text{ref}}} = 0.001\% \times \widehat{V}^i_0$. The damage function $\mathcal{D}$ is defined in (18).

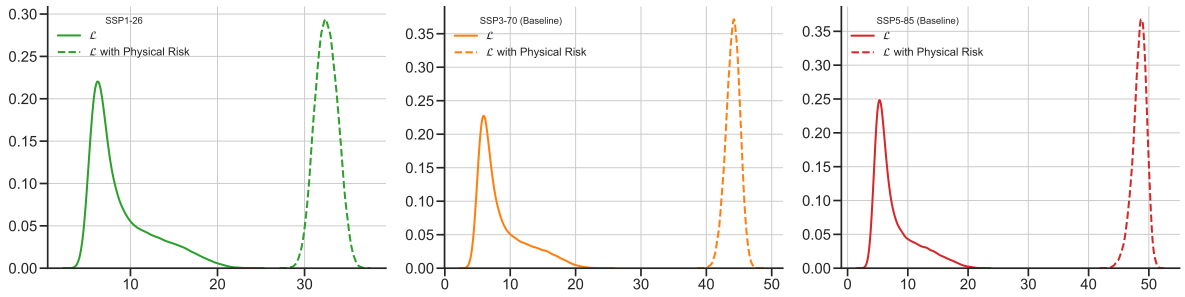

Figure 8: Portfolio losses with and without physical risk when $t = 5$ years for the scenarios SSP1-26, SSP3-70, and SSP5-85.

As anticipated, incorporating a physical risk term significantly shifts the portfolio loss distribution upward. In the subsequent numerical tests assessing the accuracy of PCA-PCE approximations, we eliminate physical risk by setting $\mathrm{EPD}^i(t) = 0$ for all i, and focus solely on the transition risk component.

5.4.2 PCA approximation

We now evaluate the PCA approximation. In Figure 9, we present the density plots of the loss portfolio and the two-factor-PCA-approximated loss. As anticipated from the analysis in Section 5.2, the PCA approximation is highly accurate, with the two densities appearing virtually identical.

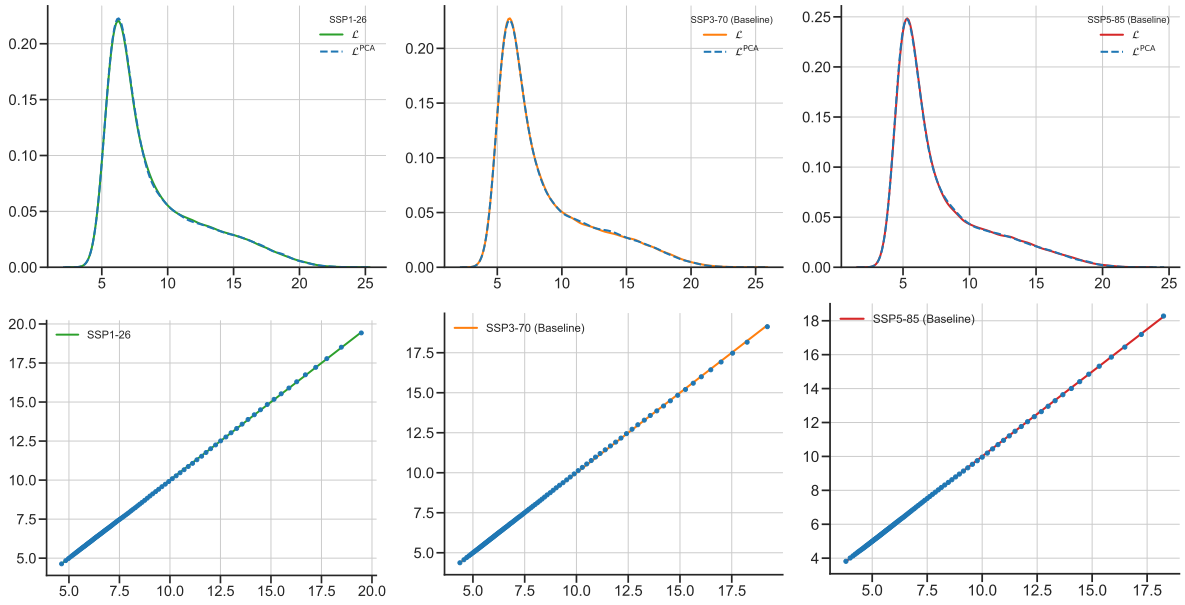

Figure 9: Portfolio loss $\mathcal{L}$ and two-factor-PCA-approximated loss $\mathcal{L}^{\text{PCA}}$ when $t = 5$ years for the scenarios SSP1-26, SSP3-70, and SSP5-85 (top figures) and associated Q-Q plots (bottom figures).

5.4.3 PCA-PCE approximation

Next, we assess the PCA-PCE-approximated loss for truncation parameters $M \in \{1, 3, 5, 10\}$ along with the respective Q-Q plot. As expected, the approximation improves with higher values of M.

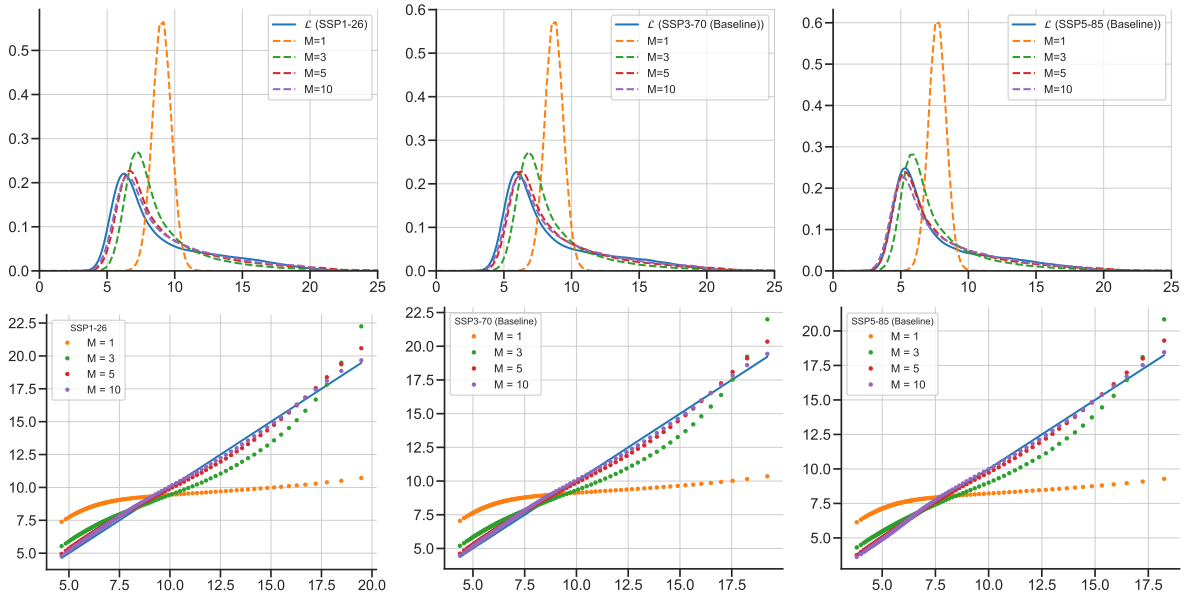

Figure 10: Comparison of $\mathcal{L}$ and $\mathcal{L}^{\text{PCA,PCE,G}}$ (left figures) and associated Q-Q plots (right figures) with $M = 1, 3, 5$ and 10 when $t = 5$ years for the scenarios SSP1-26, SSP3-70, and SSP5-85.

Let us further describe the numerical implementations of our PCA-PCE approximation for the portfolio loss $\mathcal{L}$. We assume that all parameters listed in Table 3 are available.

For each scenario, we begin by pre-computing the PCA decomposition of the covariance matrix K_X, see (26), along with the mean and covariance of the vector ε for the PCE. Next, we

perform a Monte Carlo simulation to obtain n_{mc} samples of the approximated loss $\mathcal{L}^{\text{PCA,PCE}}$, as described in Algorithm 2.

As an example, when $n = 10,000$ obligors and $n_{\text{mc}} = 10^5$ Monte Carlo samples, Algorithm 1 takes approximately 75 seconds, while Algorithm 2 takes approximately 2 seconds. For both Algorithms, the pre-computation of $L^i(t)$ and $\widehat{\gamma}_t^i$ takes about 10 minutes.

Algorithm 1: Crude Monte Carlo: Sampling of the portfolio loss $\mathcal{L}_t$

Output: n_{mc} i.i.d. samples of $\mathcal{L}_t$;
for $j \leftarrow 1$ **to** n_{mc} **do**
  Compute vector of optimal emissions $(\widehat{\gamma}_t^1, \dots, \widehat{\gamma}_t^n)$, see Theorem 4;
  Sample Gaussian vector $(\widehat{p}_t^1, \dots, \widehat{p}_t^n)$, see (22) and (23);
  Compute vector of optimal values $(\widehat{V}_t^1, \dots, \widehat{V}_t^n)$ where $\widehat{V}^i(t) = h^i(t, \widehat{p}_t^i)$, see (25);
  Compute the portfolio loss $\mathcal{L}_t = \sum_{i=1}^n \Lambda^i \times \mathbf{1}_{\left\{\widehat{V}_t^i \le L^i(t)\right\}}$, see (24).
end

Algorithm 2: Monte Carlo: Sampling of the PCA-PCE portfolio loss with Gaussian approximation (with loss functions as in Example 1)

Output: n_{mc} i.i.d. samples of $\mathcal{L}_t^{\text{PCA,PCE,G}}$;
Offline computation:
Find PCA decomposition of the covariance matrix K_{X_t}, see Section 5.2;
Compute parameters $\mathcal{M}, \mathcal{K}$ (33) for the PCE using recursive relations in Proposition 9;
for $j \leftarrow 1$ **to** n_{mc} **do**
  Sample $\left(\varepsilon^{\text{G}}_{n,m_1,m_2}\right)_{m_1+m_2=m,\, 0\le m\le M} \sim \mathcal{N}(\mathcal{M}, \mathcal{K})$;
  Sample two independent $G^1, G^2 \sim \mathcal{N}(0,1)$;
  Compute PCA-PCE portfolio loss with Gaussian approximation $\mathcal{L}_t^{\text{PCA,PCE,G}} = \sum_{m=0}^M \sum_{\substack{m_1,m_2\ge 0\\ m_1+m_2=m}} \varepsilon^{\text{G}}_{n,m_1,m_2} \text{He}_{m_1}(G^1)\text{He}_{m_2}(G^2)$, see (32);
end

Remark 6. To calibrate the default boundary $L^i(t)$, we proceed as in [5, Section 3.2.]. Given a default intensity rate λ^i_{ref} for the ith obligor, $L^i(t)$ is determined such that

$$\mathbb{P}\left(\widehat{V}_t^i(\omega_1 = \omega_2 = 0) \le L^i(t)\right) = 1 - e^{-\lambda^i_{\text{ref}}\, t},$$

where $\widehat{V}_t^i(\omega_1 = \omega_2 = 0)$ corresponds to the optimal obligor's value with no reward or penalization.

Remark 7 (Projected gradient descent to compute $\widehat{\gamma}^i_{\bullet,t}$ under the setting of Theorem 2)**.** In general, there is no closed-form solution for the optimal emissions. To numerically solve

$$\arg\max_{\gamma_\bullet \in \mathcal{G}^i_{\bullet,t}} f_t^i(\gamma_\bullet), \tag{34}$$

we can use a projected gradient descent (PGD) [8]. More precisely, we first use gradient descent and then perform a projection onto $\mathcal{G}^i_{\bullet,t}$, see (6). At the k^{th} iteration, we set for each energy source $\mathsf{e} \in \mathscr{E}^i$,

$$\gamma^{i,(k+1)}_{\mathsf{e},t} = \text{Proj}_{[0,\lambda^{\max}_{\mathsf{e},t}]}\left(\gamma^{i,(k)}_{\mathsf{e},t} - \eta_k \frac{\partial}{\partial \gamma^i_{\mathsf{e},t}} f_t^i(\gamma^{i,(k)}_{\mathsf{e},t})\right) = \left(\gamma^{i,(k)}_{\mathsf{e},t} - \eta_k \frac{\partial}{\partial \gamma^i_{\mathsf{e},t}} f_t^i(\gamma^{i,(k)}_{\mathsf{e},t})\right)^+ \wedge \lambda^{\max}_{\mathsf{e},t},$$

where η_k is the step-size.

Recall from [24, Section 2.1] that if g is a convex and L-smooth function on $\mathbb{R}^d$ then the convergence rate for a gradient descent $\gamma^{(k)} = \gamma^{(k-1)} - \eta_k \nabla g(\gamma^{(k-1)})$ is $g(\gamma^{(k)}) - g(\widehat{\gamma}) \le \mathcal{O}(1/k)$.

If in addition g is μ-strongly convex [7], $g(\gamma^{(k)}) - g(\widehat{\gamma}) \leq \mathcal{O}((1-\mu/L)^k) = \mathcal{O}(e^{-k(\mu/L)})$ where k is the number of iterations. Because the projection is onto a closed convex set, the convergence rates remain the same for (34), see [24, Section 2.2.5].

Defining $A := -x_\bullet \cdot D^2 f_t(\gamma_\bullet) x_\bullet$, we observe that:

$$A = 2\Big(\sum_{\mathsf{e}\in\mathscr{E}} \beta^\theta_{\mathsf{e},t} x_\mathsf{e}^2 - \omega_2 \big(\sum_{\mathsf{e}\in\mathscr{E}} x_\mathsf{e}\big)^2\Big) \geq 2\Big(\sum_{\mathsf{e}\in\mathscr{E}} \beta^\theta_{\mathsf{e},t} x_\mathsf{e}^2 \Big(1 - \omega_2 \sum_{\mathsf{e}\in\mathscr{E}} \frac{1}{\beta^\theta_{\mathsf{e},t}}\Big)\Big) \geq \mu \sum_{\mathsf{e}\in\mathscr{E}} x_\mathsf{e}^2,$$

where $\mu = 2\min_{\mathsf{e}'\in\mathscr{E}^i} \beta^\theta_{\mathsf{e}',t}\Big(1-\omega_2 \sum_{\mathsf{e}\in\mathscr{E}} \frac{1}{\beta^\theta_{\mathsf{e},t}}\Big)$. Similarly, $A \leq L \sum_{\mathsf{e}\in\mathscr{E}} x_\mathsf{e}^2$ with $L = 2\max_{\mathsf{e}\in\mathscr{E}^i} \beta_{\mathsf{e},t}$. Consequently, $-f_t(\cdot)$ is convex, L-smooth, and μ-strongly convex, which ensures that a PGD has the exponential convergence rate $\mathcal{O}(e^{-k(\mu/L)})$.

6 Conclusion

We have designed an end-to-end methodology to assess the credit risk of a large portfolio of obligors impacted by transition and physical climate risks, addressing both modeling and computational challenges. Our model takes as input an SSP scenario, transforms it into an optimal emission strategy for each obligor based on its characteristics, and then deduces the impact on the obligor's firm value within a structural credit modeling framework. The aggregation of individual losses across the large portfolio is achieved using two dimension-reduction techniques–Principal Component Analysis and Polynomial Chaos Expansion–proven to be efficient and accurate. In the near future, we will apply the whole procedure to real data.

References

[1] S. Asmussen and H. Albrecher. *Ruin Probabilities*. World Scientific, 2010.

[2] Basel Committee on Banking Supervision. Climate-related risk drivers and their transmission channels. *Bank for International Settlements*, d517, 2021. https://www.bis.org/bcbs/publ/d517.htm.

[3] S. Battiston, A. Mandel, I. Monasterolo, and A. Roncoroni. Climate Credit Risk and Corporate Valuation. *Available at SSRN 4124002*, 2023. https://papers.ssrn.com/sol3/papers.cfm?abstract_id=4124002.

[4] T. R. Bielecki, S. Crépey, and M. Jeanblanc. Up and down credit risk. *Quantitative Finance*, 10(10):1137–1151, 2010.

[5] F. Bourgey, E. Gobet, and Y. Jiao. Bridging socioeconomic pathways of CO2 emission and credit risk. *Annals of Operations Research*, 336:1197–1218, 2024.

[6] F. Bourgey, E. Gobet, and C. Rey. Metamodel of a Large Credit Risk Portfolio in the Gaussian Copula Model. *SIAM Journal on Financial Mathematics*, 11(4):1098–1136, 2020.

[7] F. Bourgey, E. Gobet, and C. Rey. A Comparative Study of Polynomial-Type Chaos Expansions for Indicator Functions. *SIAM/ASA Journal on Uncertainty Quantification*, 10(4):1350–1383, 2022.

[8] P. H. Calamai and J. J. Moré. Projected gradient methods for linearly constrained problems. *Mathematical Programming*, 39(1):93–116, 1987.

[7] A differentiable function $f : \mathbb{R}^d \to \mathbb{R}$ is L-smooth if $f(y) \leq f(x) + \nabla f(x)\cdot(y-x) + \frac{L}{2}\|y-x\|^2$ and is μ-strongly convex with $\mu > 0$ if $f(y) \geq f(x) + \nabla f(x)\cdot(y-x) + \frac{\mu}{2}\|y-x\|^2$ for all $x, y \in \mathbb{R}^d$.

[9] M. Carney. Breaking the tragedy of the horizon–climate change and financial stability. *Speech given at Lloyd's of London*, 29:220–230, 2015.

[10] F. Cucker and S. Smale. On the Mathematical Foundations of Learning. *Bulletin of the American Mathematical Society*, 39(1):1–49, 2002.

[11] J. Garnier, J. Gaudemet, and A. Gruz. The Climate Extended Risk Model (CERM). *Preprint arXiv:2103.03275*, 2021.

[12] D. R. Gómez, J. Wattersson, B. Americano, C. Ha, G. Marland, E. Matsika, L. Namayanga, B. Osman, J. Saka, and K. Treanton. Stationary combustion. *Energy, 2006 IPCC Guidelines for National Greenhouse Gas Emissions Inventories, Intergovernmental Panel on Climate Change, Geneva*, 2006. https://www.ipcc-nggip.iges.or.jp/public/2006gl/pdf/2_Volume2/V2_2_Ch2_Stationary_Combustion.pdf.

[13] M. B. Gordy. A risk-factor model foundation for ratings-based bank capital rules. *Journal of Financial Intermediation*, 12(3):199–232, 2003.

[14] P. H. Howard and T. Sterner. Few and Not So Far Between: A Meta-analysis of Climate Damage Estimates. *Environmental and Resource Economics*, 68(1):197–225, 2017.

[15] International Energy Agency. Emissions factors 2022. *IEA website*, 2023. https://www.iea.org/data-and-statistics/data-product/emissions-factors-2022.

[16] IPCC. Summary for policymakers. In V. Masson-Delmotte, P. Zhai, H.-O. Pörtner, D. Roberts, J. Skea, P. Shukla, A. Pirani, W. Moufouma-Okia, C. Péan, R. Pidcock, S. Connors, J. Matthews, Y. Chen, X. Zhou, M. Gomis, E. Lonnoy, T. Maycock, M. Tignor, , and T. Waterfield, editors, *Global warming of 1.5 °C. An IPCC Special Report on the impacts of global warming of 1.5 °C above pre-industrial levels and related global greenhouse gas emission pathways, in the context of strengthening the global response to the threat of climate change, sustainable development, and efforts to eradicate poverty*. World Meteorological Organization, Geneva, Switzerland, 2018.

[17] J. F. C. Kingman. *Poisson Processes*, volume 3 of *Oxford Studies in Probability*. The Clarendon Press Oxford University Press, New York, 1993. Oxford Science Publications.

[18] D. Lando. On Cox Processes and Credit Risky Securities. *Review of Derivatives Research*, 2:99–120, 1998.

[19] T. Le Guenedal and P. Tankov. Corporate debt value under transition scenario uncertainty. *To appear in Mathematical Finance*, 2024. https://papers.ssrn.com/sol3/papers.cfm?abstract_id=4152325.

[20] A. Lefevre and A. Tourin. Incorporating Climate Risk into Credit Risk Modeling: An Application in Housing Finance. *FinTech*, 2(3):614–640, 2023.

[21] D. X. Li. On default correlation: A copula function approach. *The Journal of Fixed Income*, 9(4):43–54, 2000.

[22] M. Malte, Z. R. J. Nicholls, J. Lewis, M. J. Gidden, E. Vogel, M. Freund, U. Beyerle, C. Gessner, A. Nauels, N. Bauer, J. G. Canadell, J. S. Daniel, A. John, P. B. Krummel, G. Luderer, N. Meinshausen, S. A. Montzka, P. J. Rayner, S. Reimann, S. J. Smith, M. van den Berg, G. J. M. Velders, M. K. Vollmer, and R. H. J. Wang. The shared socio-economic pathway (SSP) greenhouse gas concentrations and their extensions to 2500. *Geoscientific Model Development*, 13:3571–3605, 2020.

[23] A. J. McNeil and R. Frey. Dependent defaults in models of portfolio credit risk. *Journal of Risk*, 6:59–92, 2003.

[24] Y. Nesterov. *Lectures on Convex Optimization*, volume 137. Springer, 2018.

[25] W. Nordhaus and P. Sztorc. DICE 2013R Introduction and user's manual. *Yale University and the National Bureau of Economic Research, USA*, 2013. http://acdc2007.free.fr/dicemanual2013.pdf.

[26] W. D. Nordhaus. An optimal transition path for controlling greenhouse gases. *Science*, 258(5086):1315–1319, 1992.

[27] F. W. Olver. *NIST Handbook of Mathematical Functions hardback and CD-ROM*. Cambridge University Press, 2010.

[28] R. K. Pachauri, A. Reisinger, et al. IPCC fourth assessment report. *IPCC, Geneva*, 2007:044023, 2007. https://archive.ipcc.ch/publications_and_data/ar4/wg1/en/ch2s2-10-2.html.

[29] K. Riahi, D. P. van Vuuren, E. Kriegler, J. Edmonds, B. C. O'Neill, S. Fujimori, N. Bauer, K. Calvin, R. Dellink, O. Fricko, W. Lutz, A. Popp, J. C. Cuaresma, S. KC, M. Leimbach, L. Jiang, T. Kram, S. Rao, J. Emmerling, K. Ebi, T. Hasegawa, P. Havlik, F. Humpenöder, L. A. D. Silva, S. Smith, E. Stehfest, V. Bosetti, J. Eom, D. Gernaat, T. Masui, J. Rogelj, J. Strefler, L. Drouet, V. Krey, G. Luderer, M. Harmsen, K. Takahashi, L. Baumstark, J. C. Doelman, M. Kainuma, Z. Klimont, G. Marangoni, H. Lotze-Campen, M. Obersteiner, A. Tabeau, and M. Tavoni. The Shared Socioeconomic Pathways and their energy, land use, and greenhouse gas emissions implications: An overview. *Global Environmental Change*, 42:153–168, jan 2017.

[30] H. Ritchie, M. Roser, and P. Rosado. Energy. *Our World in Data*, 2022. https://ourworldindata.org/energy.

[31] T. Roncalli. *Handbook of Financial Risk Management*. CRC Press, 2020.

[32] S. Schlömer, T. Bruckner, L. Fulton, E. Hertwich, A. McKinnon, D. Perczyk, J. Roy, R. Schaeffer, R. Sims, P. Smith, et al. Annex III: Technology-specific cost and performance parameters. In *Climate change 2014: Mitigation of climate change: Contribution of Working Group III to the fifth assessment report of the Intergovernmental Panel on Climate Change*, pages 1329–1356. Cambridge University Press, 2014. https://www.ipcc.ch/site/assets/uploads/2018/02/ipcc_wg3_ar5_annex-iii.pdf.

[33] S. Seneviratne, X. Zhang, M. A. abd W. Badi, C. Dereczynski, A. D. Luca, S. Ghosh, I. Iskandar, J. Kossin, S. Lewis, F. Otto, I. Pinto, M. Satoh, S. Vicente-Serrano, M. Wehner, and B. Zhou. Weather and climate extreme events in a changing climate. In V. Masson-Delmotte, P. Zhai, A. Pirani, S. Connors, C. Péan, S. Berger, N. Caud, Y. Chen, L. Goldfarb, M. Gomis, M. Huang, K. Leitzell, E. Lonnoy, J. Matthews, T. Maycock, T. Waterfield, O. Yelekci, R. Yu, and B. Zhou, editors, *Climate Change 2021: The Physical Science Basis. Contribution of Working Group I to the Sixth Assessment Report of the Intergovernmental Panel on Climate Change*, pages 1513–1766. Cambridge University Press, Cambridge, United Kingdom and New York, NY, USA, 2021.

[34] O. Vasicek. Limiting Loan Loss Probability Distribution. *KMV corporation*, 1991.

[35] M. L. Weitzman. GHG Targets as Insurance Against Catastrophic Climate Damages. *Journal of Public Economic Theory*, 14(2):221–244, 2012.

A Polynomial Chaos Expansion

For any $m \in \mathbb{N}$, denote $\mathrm{He}_m(x) := (-1)^m e^{\frac{x^2}{2}} \frac{\mathrm{d}^m}{\mathrm{d}x^m}\left(e^{-\frac{x^2}{2}}\right)$ the probabilist's Hermite polynomials. They satisfy the three-term recurrence relation

$$\mathrm{He}_0(x) = 1, \quad \mathrm{He}_1(x) = x, \quad \mathrm{He}_{m+2}(x) = x\mathrm{He}_{m+1}(x) - (m+1)\mathrm{He}_m(x), \qquad \forall m \in \mathbb{N}.$$

For a detailed account of Hermite polynomials, see [27, Chapter 18].

Proposition 8 ([7, Proposition 2.2 for Hermite polynomials]). *Let $c \in \mathbb{R}$ and $Z \in \mathbb{R}$. Then,*

$$\mathbf{1}_{c \le Z} = \sum_{m=0}^{\infty} \tau_m(c)\, \mathrm{He}_m(Z)$$

where $\tau_0(c) = \Phi(-c)$ and $\tau_m(c) = \frac{e^{-\frac{c^2}{2}}}{m!\sqrt{2\pi}}\mathrm{He}_{m-1}(c)$ for all $m \in \mathbb{N}^*$. The equality holds for all $Z \neq c$.

Proposition 9 ([6, Proposition 3.1]). *Let $a \in \mathbb{R}^*, b \in \mathbb{R}$ and $X \sim \mathcal{N}(0,1)$. For every $i, j \in \mathbb{N}$, define*

$$\begin{aligned}\mu_i(a,b) &:= \mathbb{E}\left[\tau_i(aX+b)\right],\\ \sigma_{i,j}(a,b) &:= \mathrm{Cov}\left(\tau_i(aX+b), \tau_j(aX+b)\right).\end{aligned}$$

Then, the following recursive relations hold:

$$\begin{cases}\mu_0(a,b) = \Phi\left(-\frac{b}{\sqrt{1+a^2}}\right), \qquad \mu_1(a,b) = \frac{e^{-\frac{b^2}{2(1+a^2)}}}{\sqrt{2\pi}\sqrt{1+a^2}},\\ \mu_{i+2}(a,b) = \frac{b}{(i+2)(1+a^2)}\mu_{i+1}(a,b) - \frac{i}{(i+2)(i+1)(1+a^2)}\mu_i(a,b),\end{cases}$$

$$\begin{cases}\sigma_{0,0}(a,b) = \Phi_\Sigma\left((-b,-b)^\top\right) - \mu_0(a,b)^2, \quad \Sigma = \left(\begin{smallmatrix}1+a^2 & a^2\\ a^2 & 1+a^2\end{smallmatrix}\right).\\ \sigma_{0,1}(a,b) = \mu_1(a,b)\left(\mu_0\left(\frac{a}{\sqrt{1+a^2}}, \frac{b}{1+a^2}\right) - \mu_0(a,b)\right),\\ \sigma_{0,i+2}(a,b) = \frac{b}{(i+2)(1+a^2)}\sigma_{0,i+1}(a,b) - \frac{i}{(i+1)(i+2)(1+a^2)}\sigma_{0,i}(a,b)\\ \qquad\qquad - \frac{a^2}{(i+2)(1+a^2)}\mu_1(a,b)\mu_{i+1}\left(\frac{a}{\sqrt{1+a^2}}, \frac{b}{1+a^2}\right),\\ \sigma_{i+1,j+1}(a,b) = \frac{1}{a^2(i+1)}\left[-\left(1+a^2\right)(j+2)\,\sigma_{i,j+2}(a,b) + b\sigma_{i,j+1}(a,b) - \frac{j}{j+1}\sigma_{i,j}(a,b)\right]\\ \qquad\qquad - \mu_{i+1}(a,b)\mu_{j+1}(a,b),\end{cases}$$

where for all $x \in \mathbb{R}^2$, $\Phi_\Sigma(x) := \mathbb{P}(Y \le x)$ and $Y \sim \mathcal{N}(0,\Sigma)$ with Σ positive definite.

B Proof of measurability in time for Theorem 1

We show that the (deterministic) optimal solution $\widehat{\gamma}_{\bullet,t}$ of Theorem 1 is measurable in time. Let $d = |\mathscr{E}^i|$. We use the notation $f(t,\boldsymbol{x}) : [0,+\infty) \times \mathbb{R}^d \to \mathbb{R}$ to denote the function $f_t^i(\cdot)$ defined in (8) by

$$f_t^i(\boldsymbol{x}) := \frac{\mathrm{AP}^i}{r+b^i}\, c_\bullet^{i,\theta} \cdot \boldsymbol{x} - \alpha_{\bullet,t}^{i,\theta} \cdot \boldsymbol{x} - \beta_{\bullet,t}^{i,\theta} \cdot \boldsymbol{x}^2 - \ell_1^i\left(\mathbf{1}\cdot\boldsymbol{x} - \widetilde{\gamma}_t^i\right) + \ell_2^i\left(\widetilde{\gamma}_t^i - \mathbf{1}\cdot\boldsymbol{x}\right)$$

where for any $\boldsymbol{x} = (x_1, \cdots, x_d)$, the notation $\boldsymbol{x}^2$ denotes the vector $(x_1^2, \cdots, x_d^2)$. The standing assumptions are

1. For any $\boldsymbol{x} \in \mathbb{R}^d$, $f(\cdot,\boldsymbol{x}) : \mathbb{R}^+ \to \mathbb{R}$ is measurable.

2. For any $t \in \mathbb{R}^+$, $f(t,\cdot) : \mathbb{R}^d \to \mathbb{R}$ is continuous.

For the sake of notational simplicity in (6), we rewrite the set $\mathcal{G}^i_{\bullet,t}$ as

$$\mathcal{G}_t := [0, \lambda_1(t)] \times \cdots \times [0, \lambda_d(t)],$$

for some measurable (in time) mappings λ_i. This is a compact subset of $\mathbb{R}^d$. We define a new function extending $f(t,\cdot)$ outside $\mathcal{G}_t$ as

$$g : \begin{cases} \mathbb{R}^+ \times \mathbb{R}^d & \to \mathbb{R}, \\ (t,x) & \mapsto f(t,\boldsymbol{x})\mathbf{1}_{\boldsymbol{x}\in\mathcal{G}_t} - \infty \mathbf{1}_{\boldsymbol{x}\notin\mathcal{G}_t} \end{cases}.$$

Since the λ_i's are measurable, the indicator functions are measurable in time (for any given $\boldsymbol{x} \in \mathbb{R}^d$), and since $f(\cdot,\boldsymbol{x})$ is measurable too, $g(\cdot,\boldsymbol{x})$ is measurable in time. Owing to the form of $\mathcal{G}_t$ and the continuity of f in the second variable, observe that

$$\widehat{f}(t) := \max_{\boldsymbol{x}\in\mathcal{G}_t} f(t,\boldsymbol{x}) = \sup_{\boldsymbol{x}\in\mathbb{Q}} g(t,\boldsymbol{x}).$$

As a countable supremum of measurable functions, $\widehat{f}$ is a measurable mapping.

Now, denote by $\boldsymbol{x}^*_t \in \mathcal{G}_t$ the point that maximizes $f(t,\cdot)$ on $\mathcal{G}_t$. Let us show that $\mathcal{T} := \{t \in \mathbb{R}^+ : \boldsymbol{x}^*_t \leq \bar{\boldsymbol{x}}\}$ is a measurable set for any given $\bar{\boldsymbol{x}} \in \mathbb{R}^d$. Observe that

$$\mathcal{T} = \bigcap_{m=1}^{\infty} \bigcup_{\boldsymbol{x}\in\mathbb{Q},\boldsymbol{x}\leq\bar{\boldsymbol{x}}} \Big\{ g(t,\boldsymbol{x}) \geq \widehat{f}(t) - \frac{1}{m} \Big\},$$

i.e., $\mathcal{T}$ is a countable intersection of countable unions of measurable sets, thus it is a measurable set. □

C Model parameters

Global Variables	**Notation**
Number of obligors	$n \in \mathbb{N}^*$
Truncation parameter in the PCE	$M \in \mathbb{N}^*$
Emission trajectory (e.g., SSP). Unit: $\mathtt{CO_2e}$	$t \mapsto \widetilde{\gamma}_t$
Atmospheric temperature trajectory	$t \mapsto \mathcal{T}_{\mathrm{ATM}}(t)$
All energy sources available	$\mathscr{E}^{\mathrm{all}}$
Discount factor	$r > 0$
The reference time for the physical risk calibration	t_{ref}
Portfolio loss	$\mathcal{L}$
Portfolio loss with rank-two PCA approximation	$\mathcal{L}^{\mathrm{PCA}}$
Portfolio loss with rank-two PCA and PCE approximations	$\mathcal{L}^{\mathrm{PCA,PCE}}$
Portfolio loss with rank-two PCA, PCE, and Gaussian approximations	$\mathcal{L}^{\mathrm{PCA,PCE,G}}$
Variables specific to the ith obligor	**Notation**
Energy sources available	$\mathscr{E}^i$
Vector of optimal GHG emissions at time t	$\gamma^i_{\bullet,t} = (\gamma_{\mathtt{e},t})_{\mathtt{e}\in\mathscr{E}^i}$
Optimal log production at time t	$\widehat{p}^i_t$
Optimal obligor's value at time t	$\widehat{V}^i_t$
Penalization and reward function	$\ell^i_1(\cdot)$ and $\ell^i_2(\cdot)$
Penalty and reward coefficients	ω^i_1 and ω^i_2
Systemic and idiosyncratic risk factors	B and B^i
Correlation to the systemic factor	ρ^i
Average production level	a^i
Mean-reverting parameter	b^i
Dependence of the obligor's energy consumption on $\mathtt{e}$	$c^i_{\mathtt{e}}$
Average price	AP^i
Profit function	$\pi^i(\cdot)$
Vector of prices per unit of all $\mathtt{e}$-energies consumed at time t	$\alpha^i_{\bullet,t} = (\alpha^i_{\mathtt{e},t})_{\mathtt{e}\in\mathscr{E}^i}$
	$\beta^i_{\bullet,t} = (\beta^i_{\mathtt{e},t})_{\mathtt{e}\in\mathscr{E}^i}$
Vector of power/$\mathtt{CO_2e}$ ratio for all $\mathtt{e}$-energies. Unit: $\mathtt{kW/kgCO_2e}$	$\theta^i_{\bullet,t} = (\theta^i_{\mathtt{e},t})_{\mathtt{e}\in\mathscr{E}^i}$
Product of loss given default and exposure at default	Λ^i
Poisson process associated to weather event $\mathtt{cw}$ and geographical zone l at time t	$N^{i,\mathtt{cw},l}_t$
Corresponding Poisson intensity and loss	$\lambda^{i,\mathtt{cw},l}_t$ and $Z^{i,\mathtt{cw},l}_t$
Expected physical damage at time t	$\mathrm{EPD}^i(t)$
Default barrier at time t	$L^i(t)$

Table 3: List of notations for the model parameters.